Fisheries and Oceans Canada | Pêches et Océans Canada
Ecosystems and Oceans Science | Sciences des écosystèmes et des océans

Canadian Science Advisory Secretariat (CSAS)

Research Document 2019/008

Newfoundland and Labrador Region

Analysis of the Variability of the Ocean Currents in the Coast of Bays Area

A.W. Ratsimandresy, S. Donnet, S. Snook, and P. Goulet

Science Branch
Fisheries and Oceans Canada
80 East White Hills Road
PO Box 5667, St. John's NL A1C 5X1

June 2019

Canada

Foreword

This series documents the scientific basis for the evaluation of aquatic resources and ecosystems in Canada. As such, it addresses the issues of the day in the time frames required and the documents it contains are not intended as definitive statements on the subjects addressed but rather as progress reports on ongoing investigations.

Published by:

Fisheries and Oceans Canada
Canadian Science Advisory Secretariat
200 Kent Street
Ottawa ON K1A 0E6

http://www.dfo-mpo.gc.ca/csas-sccs/
csas-sccs@dfo-mpo.gc.ca

ISSN 1919-5044

Correct citation for this publication:

Ratsimandresy, A.W., Donnet, S., Snook, S., and P. Goulet. 2019. Analysis of the variability of the ocean currents in the Coast of Bays area. DFO Can. Sci. Advis. Sec. Res. Doc. 2019/008. viii + 59 p.

Aussi disponible en français :

Ratsimandresy, A.W., Donnet, S., Snook, S., et P. Goulet. 2019. Analyse de la variabilité des courants océaniques dans la région de Coast of Bays. Secr. can. de consult. sci. du. MPO, Doc. de. rech. 2019/008. viii + 61 p.

TABLE OF CONTENTS

LIST OF TABLES IV

LIST OF FIGURES IV

LIST OF ACRONYMS VII

ABSTRACT VIII

INTRODUCTION 1

INSTRUMENTATION, DATA, AND METHODOLOGY 2

- DATA COLLECTION AND REDUCTION 2
- DATA ANALYSIS 4
  - Summary Statistics 4
  - Current velocity analysis 4
  - Tidal Analysis 5

RESULTS 10

- TIMESERIES OF CURRENTS IN THE COAST OF BAYS AREA 10
- ANALYSIS OF CURRENT SPEED 11
  - Median current speed 11
  - Maximum recorded current speed 12
  - Spread of the current speed 12
  - Temporal variability 19
- CURRENT VELOCITY ANALYSIS 25
  - Hermitage Bay – Bay D'Espoir 25
  - Belle Bay 26
  - Connaigre Peninsula 26
- TIDES 34

DISCUSSION 42

CONCLUSION AND RECOMMENDATION 45

ACKNOWLEDGMENTS: 46

REFERENCES CITED 47

APPENDIX I 51

APPENDIX II 55

APPENDIX III 56

APPENDIX IV 57

APPENDIX V 59

LIST OF TABLES

Table 1: Summary of the ADCP current data collected in the Coast of Bays area between 2009 and 2014. 3

Table 2: Summary (mean and standard deviation) of the major tidal constituents in the Coast of Bays area computed with the ADCP pressure sensor, average amplitude (cm) and phase (degrees). 34

Table 3: Maximum tidal current speeds [cm/s] for the major constituents computed using vertically averaged currents. 38

LIST OF FIGURES

Figure 1. Coast of Bays study area showing the different areas of interest: Hermitage Bay, Bay d'Espoir, Belle Bay, Connaigre Bay, Harbour Breton, Northeast Arm, and Great Bay de l'Eau. The figure also illustrates the location of the aquaculture licences (red and blue dots) in the Coast of Bays (as of November 2015; source: Department of Fisheries and Aquaculture 2015). Detailed map of specific areas with names used in the present document are given in the lower panels. 6

Figure 2. ADCP mooring configuration. 7

Figure 3. ADCP stations in the Coast of Bay area. 8

Figure 4. Depth of the first cell measurement (top panel), height above bottom, hab, of the deepest measured cell (mid panel), percentage water column coverage (bottom panel) of the analyzed ocean currents timeseries. 9

Figure 5. 15 days (1 Jul. 2011 - 16 Jul. 2011) time series of current speed (upper panel) and current direction (lower panel) for station BB008 located in Belle Bay. 10

Figure 6. Current roses showing the distribution of current speed and direction at 7.5 m (left panel) and 50.5 m depth (right panel) at station BB008 for the whole measurement period (8 May 2011 to 24 Oct. 2011). Each segment illustrates the direction toward which the currents flow. 11

Figure 7. Median current speed [cm/s] in the upper layer for the Coast of Bays region. 14

Figure 8. Median current speed [cm/s] in the lower layer for the Coast of Bays region. 14

Figure 9. Maximum current speed [cm/s] recorded in the upper layer. 15

Figure 10. Maximum current speed [cm/s] recorded in the lower layer. 15

Figure 11. Box and whisker plot of the current speed in the upper layer (above 20m) for data measured in HB-BDE. The plot provides information on median and interquartile range (IQR) of data, current speeds above the upper fence (values above 1.5xIQR from the third quartile) are represented with open circles. 16

Figure 12. Box and whisker plot of the current speed in the lower layer (below 20m) for data measured in HB-BDE (analogous to Figure 11). 16

Figure 13. Box and whisker plot of the current speed in the upper layer (above 20m) for data measured in BB (analogous to Figure 11). 17

Figure 14. Box and whisker plot of the current speed in the lower layer (below 20m) for data measured in BB (analogous to Figure 11). 17

Figure 15. Box and whisker plot of the current speed in the upper layer (above 20m) for data measured in CP (analogous to Figure 11). 18

Figure 16. Box and whisker plot of the current speed in the lower layer (below 20m) for data measured in CP (analogous to Figure 11). 18

Figure 17. Seasonal variability of the median currents (cm/s) in the upper layer for Spring, Summer, and Fall. 20

Figure 18. Seasonal variability of the maximum current speed (cm/s) in the upper layer for Spring, Summer, and Fall. 21

Figure 19. Seasonal variability of the median currents (cm/s) in the lower layer for Spring, Summer, and Fall. 22

Figure 20. Seasonal variability of the maximum current speed (cm/s) in the lower layer for Spring, Summer, and Fall. 23

Figure 21. Example of monthly variability of current speed in the upper layer for stations (A) BDE19 in BDE, (B) BB008 in BB, and (C) CB006 in CB. 25%, median, and 75% represent the 25, 50, and 75 percentiles, upper fence is the value as described in the methodology on summary statistics and Max is the maximum recorded current speed. 24

Figure 22. Mean currents in the upper layer (top panel) and lower layer (bottom panel) for HB-BDE. 28

Figure 23. Maximum currents recorded in HB-BDE for the upper layer (top panel) and for the lower layer (bottom panel). 29

Figure 24. Mean currents in the upper layer (left panel) and lower layer (right panel) for BB region. Dots any current arrow means data were not available. Note the change of scale for BB currents. 30

Figure 25. Maximum currents recorded in Belle Bay for the upper layer (left panel) and for the lower layer (right panel). 31

Figure 26. Mean currents in the upper layer (top panel) and lower layer (bottom panel) for CP region. 32

Figure 27. Maximum currents recorded in Connaigre Peninsula for the upper layer (top panel) and for the lower layer (bottom panel). 33

Figure 28. Amplitude [cm] and phase (°) of the main tidal constituents computed from ADCP pressure sensor. 35

Figure 29. Amplitude in cm (top panel) and phase in degree (bottom panel) of the M2 tides computed from pressure sensor included within the ADCP. 36

Figure 30. Percentage tidal contribution to sea level variability. 37

Figure 31. Maximum current speed [cm/s] for M2 tidal currents computed from the vertically averaged currents. 38

Figure 32. Tidal ellipse for M2 computed from the vertically averaged currents in (a) BDE, (b) CP, and (c) BB. Note the change of scale for BDE region 39

Figure 33. Percentage tidal current contribution in the upper 20 m. Upper panel represents the contribution for the West-to-East component (zonal) of the currents and lower panel the contribution for the South-to-North component (meridional) of the currents. 40

Figure 34. Percentage tidal current contribution for the lower layer (below 20 m depth).Upper panel represents the contribution for the West-to-East component (zonal) of the currents and lower panel the contribution for the South-to-North component (meridional) of the currents.....41

LIST OF ACRONYMS

Acronym	Name	Description
ADCP	Acoustic Doppler Current Profiler	Instrument used to measure water current velovities
BB	Belle Bay	Major bay of interest
BDE	Bay d'Espoir	Major bay of interest
CB	Connaigre Bay	Major bay of interest
CHS	Canadian Hydrographic Service	Federal hydrographic office (Canada)
CP	Connaigre Peninsula	Broad region encompassing Connaigre Bay, Harbour Breton- Northern Arm and Great Bay De l'Eau
GBDE	Great Bay de L'Eau	Major bay of interest in this study; also a major channel of Connaigre Peninsula region
HB-BDE	Hermitage Bay - Bay d'Espoir	Region encompassing Hermitage Bay and Bay d'Espoir
HB-NA	Harbour Breton - Northeast Arm	Major bay of interest in this study; also a major channel of Connaigre Peninsula region
IQR	Interquartile range	A measure of statistical dispersion

ABSTRACT

While of importance for processes such as transport of particles to and from aquaculture sites, little has been done to study the ocean current regime to support the aquaculture activities in the Coast of Bays, an area of the south coast of Newfoundland. To complete this gap and to understand the nearshore water circulation, Acoustic Doppler Current Profilers (ADCPs) were used to measure ocean currents in the Coast of Bays between 2009 and 2014. This work describes statistics of measured water currents and results of tidal analyses (sea level and ocean currents). The analyses were performed on two layers within the water column, namely the upper 0-20 m depth and the layer below 20 m.

Significant spatial and temporal variability of the currents was observed. Low median speeds were found in sheltered coves and higher median speed in constricted areas such as those around sills and those within narrow channels. The maximum recorded current speed at each station was generally five to ten times larger than its median speed. In the vertical, the current speed near the surface was generally higher than that at depth with median speed in the upper 20 m being more than 1.3 times that at depths below 20 m. Median current speed tended to be slightly higher in the fall compared to other seasons. The analysis of the monthly variability of the current speed shows the highest maximum current speeds happening in summer or fall months. Tidal contribution to the variance of the sea level was high (~84%) while that of the vertically averaged currents was very low (~10%) except in the upper Bay d'Espoir where it was around 25%. This suggests that in addition to the tides, other and more important forcing drive the coastal circulation in the Coast of Bays region.

This information serves as a baseline for ocean current conditions and for understanding the role of tides in driving the water circulation in the area. It also helps in assessing the potential connection among aquaculture sites and helps in the development of regulatory measures (e.g. Bay Management Areas) to ensure the sustainability of aquaculture activities in Newfoundland and Labrador.

INTRODUCTION

Understanding ocean currents is a necessity for aquaculture activities. Ocean current conditions influence processes such as the spreading of waste plumes from fish farms (Venayagamoorthy et al. 2011), boundaries of mixing zones downstream of aquaculture cages (Helsley and Kim 2005), or keeping dissolved oxygen levels close to saturation (Boghen 1995) through good flushing rates. Other effects of the ocean current and its vertical structure include an impact on the behaviour of fish within cages and the influence they have on the fish schooling structure (Oppedal et al. 2011, Johansson et al. 2014). From the point of view of cage structure, the currents can cause the sea-cage to change shape and reduce the internal volume available for fish (Lader at al. 2008) thus creating potential stress on farmed fish. Ocean currents have also been reported to play a major role in the transport of pathogens between aquaculture sites. According to studies carried out in Norway, diseases such as ISA were subject to spread between farms as the virus can be passively transported by seawater movement (Vågsholm et al 1994, Jarp and Karlsen 1997). Similar transport processes have been observed at a local scale in Scotland and the Southwest New Brunswick/Maine area (JGIWG 2000, Murray 2003, McClure et al. 2005, Gustafson et al. 2007, Page et al. 2005).

As disease transport has been a growing concern in marine aquaculture, the industry in New Brunswick together with the Province of New Brunswick have developed a Bay Management Area (BMA) policy which consists in implementing single-year-class farming and in partitioning salmon farm areas into Management Areas based on a combination of oceanographic, fish health and business considerations in order to improve fish health and ensure environmental sustainability (Chang et al. 2014). The BMAs were evaluated through calculation of zones of influence of aquaculture sites using a number of tools. One of them is a circulation model which gives tidal information in the area. In their study, tidal excursion was defined and used to delineate movement of water from a farm site to the surrounding area thereby assuming the dominance of the tides in generating the currents transporting potential pathogens (a reality in New Brunswick).

With the growth of the Newfoundland aquaculture industry, the provincial department of Fisheries and Aquaculture is implementing BMAs to better manage the industry expansion (Department of Fisheries and Aquaculture, 2014a). In Newfoundland, finfish aquaculture activities started in the mid-80s in the Bay d'Espoir region and later in Belle Bay, both within the Coast of Bays area (Figure 1 and Appendix 1) with plans to further expand (DFA, 2014a). This growth has been translated into an increase in the number of aquaculture licenses as well as the surface water area used to carry out such activities (DFA 2014b). Early guidelines for site separation in the Coast of Bays area stated that aquaculture farms should be at least 1 km apart (G. Perry., Aquaculture Management, Fisheries and Oceans Canada (DFO), NL Region, pers. Comm.) while possible interaction of aquaculture activities with other fishing activities was assessed using a 2 km radius as mentioned in the actual Aquaculture License Application form. However, defining distance will not provide a complete set of information as it is also necessary to know how long it takes for a particle (a virus for instance) to reach that distance. The distance between sites combined with the time related to life cycle of the particles of interest can be compared with current velocity to evaluate the role of passive transfer of viruses among sites when investigating disease propagation (Foreman et al. 2015). Thus, as the potential for passive transfer changes depending on the water circulation in the area, it is crucial to understand the ocean currents and the different forcing that drive the circulation. Other oceanographic measurements that can support aquaculture and its development were carried out in the area (Taylor 1975, MSRL 1980, BDE-DA 1984, de Young 1983, Richard and Hay 1984, Tlusty et al. 1999, Pepper et al. 2003 and 2004, Anderson et al. 2005, Mansour et al.

2008, Burt et al. 2012) with a focus on temperature, salinity, and/or dissolved oxygen. However, little has been done with respect to the ocean current conditions (e.g. tidal, estuarine and/or wind driven). De Young (1983) analyzed ocean currents near the mouth of Fortune Bay but with a focus on deep water circulation (below ~80 m depth) which cannot be used for near-surface aquaculture related applications at the head of bay. As part of the DFO's Program for Aquaculture Regulatory Research (PARR) funded research project to carry out oceanographic study of the South coast of Newfoundland, ocean current data were collected in the Coast of Bays area between 2009 and 2014 to help understand the nearshore water circulation. It included surface current measured using surface drifters (Ratsimandresey et al. 2012) and currents measured by Acoustic Doppler Current Profilers (ADCP).

This work is part of a series of analyses to understand the oceanographic conditions and the water exchange among the different bays of the South Coast of Newfoundland, in particular the Coast of Bays (Figure 1) where the vast majority of the salmonid aquaculture activities in the province is taking place and rapidly expanding (Department of Fisheries and Aquaculture, 2014). The result of these analyses will provide scientific advice for management decisions on sustainable aquaculture. Different physical aspects of the area have been studied including a description of the area's geography, hydrology, and oceanography with focus on tides and coastal freshwater inputs as well as bathymetry (Donnet et al. 2018a) and an analysis of the water structure in the area and its spatial and temporal variability (Donnet et al. 2018b). Other aspects of the physical oceanography of the area focusing on water circulation to delineate zones of influence associated with aquaculture activities were also investigated and will be described in further publications. The work addressed in this report will present an analysis of the ocean currents measured by the ADCP.

Statistical analysis on the currents and tidal regime (sea level and currents) are described. The information will serve as a baseline for current speed and direction and for understanding the role of tides in driving the circulation in the area. It will also be useful for the on-going coastal water circulation model development for the region, e.g. for validation purposes. The area of interest is the Coast of Bays, located between 47° and 48° N and 54.5° and 56.5° W (Figure 1). It includes three main regions that are physically distinct (Donnet et al 2018a): Hermitage Bay - Bay d'Espoir (HB-BDE) on the western side, Belle Bay (BB) region on the eastern side, and the Connaigre Peninsula (CP) in between. CP includes Connaigre Bay (CB), Harbour Breton – Northeast Arm (HB-NA) and Great Bay de l'Eau (GBDE).

The work is structured as follows. The next section provides a brief description of the instrumentation, the methodology of the analysis, and the data. The results are presented in the third section, the discussion in the fourth section, and summary of the major results with recommendations in the last section. Data used and presented in this report are available at the Government of Canada's Open Data website.

INSTRUMENTATION, DATA, AND METHODOLOGY

DATA COLLECTION AND REDUCTION

The data presented in this report were collected using a variety of Teledyne RDI Workhorse Sentinel ADCPs (300, 600 and 1200 kHz Teledyne RDI, 2011). All ADCPs were configured in an upward-looking direction and collected data using a depth cell size ranging from 0.2 to 3 m depending on instrument frequency and setup. A large majority of the deployments (78 out of a total of 84) were configured with a 1 m cell size and to result with an uncertainty (1 standard deviation) of about 1 cm/s on the current speed measurement. Eleven deployments did not provide any useful data either because of instrument failure, inappropriate setting, or obstruction

of the acoustic beam by near-static object. Thus, a total of 73 timeseries of current data were available for this work. The obstruction of the acoustic beam did not, however, affect the pressure sensor thus providing five additional timeseries of sea level data. Figure 2 illustrates the typical mooring configuration as used in the collection of data within this region. In total, data were collected from 53 stations of which 29 were in HB-BDE, 15 in BB, and 9 in CP (Figure 3); of those 53 stations, 49 had useable ocean currents data (28 in HB-BDE, 12 in BB and 9 in CP). Thirteen of the stations were revisited for multiple redeployments. More than half (30 in total) of these stations was moored in close proximity to areas which were in the active and/or planning stages of aquaculture farming. Thus, many ADCPs were deployed in the nearshore zones in sheltered coves or inlets (depending on the location of the aquaculture farm) while others were moored above sills or middle of narrow channels within the bays. The ADCPs were moored at depths between 9 to 154 m (with 50% of them in the range of 54 to 73 m depth) Data were collected throughout all four seasons with an emphasis on the spring-fall seasons (Table 1). Overall, the length of the data recording ranged from 26 to 235 days (with a median of 91 days). Information on position, date, and depth of each deployment and the corresponding Gantt chart are provided in Appendix 2.

Effort was put into collecting data for as much of the water column as possible from the depth of the ADCP to the sea-surface but inherent limitations of the instrument (side lobe interference and blanking distance) and site-specific conditions has limited the profiling range:

Table 1. Summary of the ADCP current data collected in the Coast of Bays area between 2009 and 2014.

-	Number of Stations	Total number of collection days	January	February	March	April	May	June	July	August	September	October	November	December
HB-BDE	28	3244	3	3	3	12	18	21	22	15	18	17	10	3
BB	12	1555	3	3	1	2	7	8	6	7	8	9	4	3
CP	9	1794	4	4	4	5	6	7	13	10	10	9	5	4

- side lobe interference are due to the orientation of the ADCP sensors (i.e., transducers) which results in noisy data near 'hard surfaces' such as the sea surface or bottom (Teledyne RDI, Inc., 2011). To account for this, 6% of the water column data from the surface to the ADCP depth must be rejected in theory when using instruments with a 20^{o} angle such as the ones that were used for this study. In practice, it was found that up to 10% of the water column data had to be rejected (e.g., first 5 m of the water column from the sea-surface for an ADCP located at 50 m depth).
- from the ADCP transducers to the first 'cell' of the water column being measured, a distance of no-data is present due to transducer 'ringing' noise. This distance is equal to about 2 m for a 300 kHz ADCP (Teledyne RDI, 2011). Therefore, and considering the typical mooring configuration used (Figure 2), the deepest cell possible to measure was within 4-6 m from the sea-bottom for most of the measurements.
- since ADCPs measure water currents by emitting sound waves which bounce back from moving particles present within the water column, the backscatter signal strength depends on the presence or absence of such particles. Battery depletion towards the end of a few long deployments also resulted in loss of range. When the backscatter signal falls below the instrument noise level, current velocity data from the ADCPs are erroneous and must be

removed. In total, 12 deployments were affected by this issue leading to no effective data collection above 20 m depth (Figure 4). No specific temporal or spatial patterns appear, data collected in winter, summer and in between, were equally affected by this issue. The CP region was, however, less affected as only 3 deployments were subject to this issue (about half less likely than HB-BDE and BB to be affect).

Therefore, depending on the depth at the station and the limitations listed above, some measurements were limited to 28-75% of the water column (27 deployments out of the 73 available, Appendix 2). For the most part (46 deployments), however, it was possible to obtain more than 75% of the water column at a given station and period of time. With the above limitations in mind we opted to analyze stations with at least a month of continuous data, for a given level, to ensure statistical representativeness. In addition to this temporal criterion, at least 5 m depth of data per layer was necessary to calculate statistics of that layer.

Data were extracted, processed and quality controlled using a combination of factory software as well as in-house programs combined with other plotting and analysis tools.

DATA ANALYSIS

Summary Statistics

Statistical analysis was performed on the measured current speed taking into consideration two water layers: the 'upper layer' which is defined as the layer found from the closest record to the surface down to 20 m depth, and the 'lower layer' which extends from 20 m to the depth of the instrument. The upper 20 m depth range was used for its direct relevance to fish farming activities which typically utilize fish cages of 15-20 meters in height as well as for being the layer where pycnocline is generally observed (Donnet et al. 2018b). All data records within the layer of consideration were combined as one dataset and used to compute the statistical values.

The median and the maximum recorded current speed are examined and box and whisker plots (Statistics Canada 2013) were generated to provide information on the spread. The plot presents a summary of the data which includes the different quartiles, the interquartile range (IQR), as well as the lower and upper fences. The lower and upper fences represent the range of current speed without the extreme data considered as outliers (Upton & Cook, 1996). To calculate this range the IQR, defined as the difference between the first quartile (Q1, 25 percentile) and third quartile (Q3, 75 percentile), is first computed. The lower fence (LF) and upper fence (UF) is then calculated using the following formulae (Upton & Cook, 1996):

$$LF = Q1 - 1.5 * IQR \qquad UF = Q3 + 1.5 * IQR$$

In order to evaluate the seasonal variability of the ocean currents in the region, similar statistics were performed by grouping stations by season. Seasons are defined as winter (January-March), spring (April-June), summer (July-September), and fall (October-December) following Petrie et al. climatology studies for Atlantic Canada (1996a and 1996b). Data from stations with multiple deployments and with collection longer than few months period were also grouped by month and monthly statistics were computed in order to assess monthly variability.

Current velocity analysis

Current vectors were analyzed to provide statistical information on the current speed and direction and thus, information on the circulation. This was performed by computing the mean and maximum currents, the former being the vector average for each ADCP time series and the latter representing the maximum current speed and associated direction recorded during the measurement for each depth from the surface to the depth of the ADCP. Similar to the above

“summary statistics” analysis, mean and maximum currents were computed for the same two separate layers (0-20 m and 20 to bottom).

Tidal Analysis

Tidal analysis was performed on the pressure and current data using the analysis routine developed by Foreman et al. (2009). This routine gives the possibility of analyzing irregularly sampled data or data with missing measurements. The method entails embedding of nodal and astronomical argument corrections and multiple inference calculations into an overdetermined matrix that is solved using singular value decomposition technics (Golub and Van Loan 1983; Press et al. 1992). Since the tool does not provide automatic selection of the tidal constituents, 13 constituents were selected namely Z0, Q1, O1, K1, MU2, N2, M2, S2, MK3, SK3, S4, 2SM6, and M8; in addition, P1 and K2 were inferred from K1 and S2.

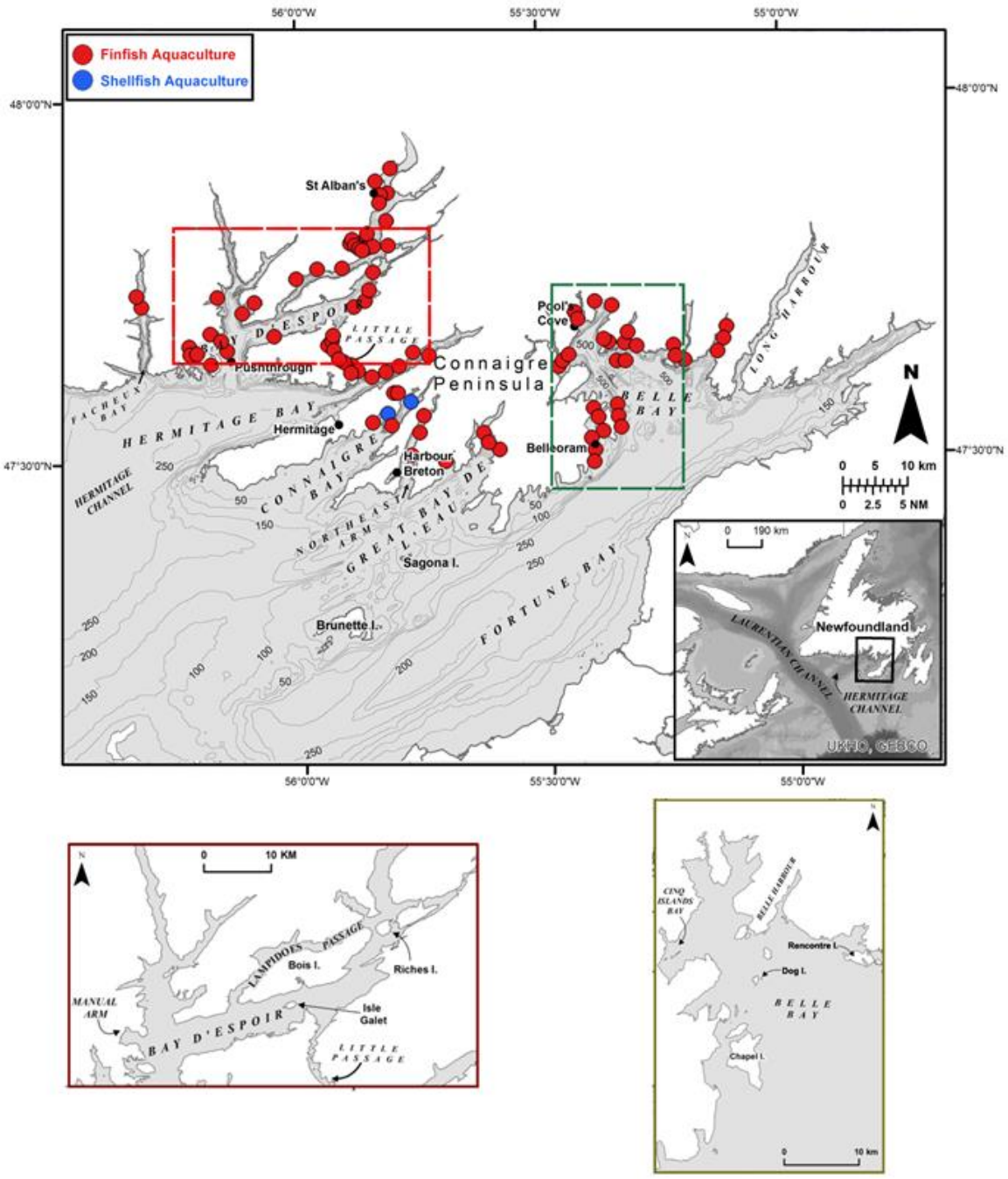

Figure 1. Coast of Bays study area showing the different areas of interest: Hermitage Bay, Bay d'Espoir, Belle Bay, Connaigre Bay, Harbour Breton, Northeast Arm, and Great Bay de l'Eau. The figure also illustrates the location of the aquaculture licences (red and blue dots) in the Coast of Bays (as of November 2015; source: Department of Fisheries and Aquaculture 2015). Detailed map of specific areas with names used in the present document are given in the lower panels.

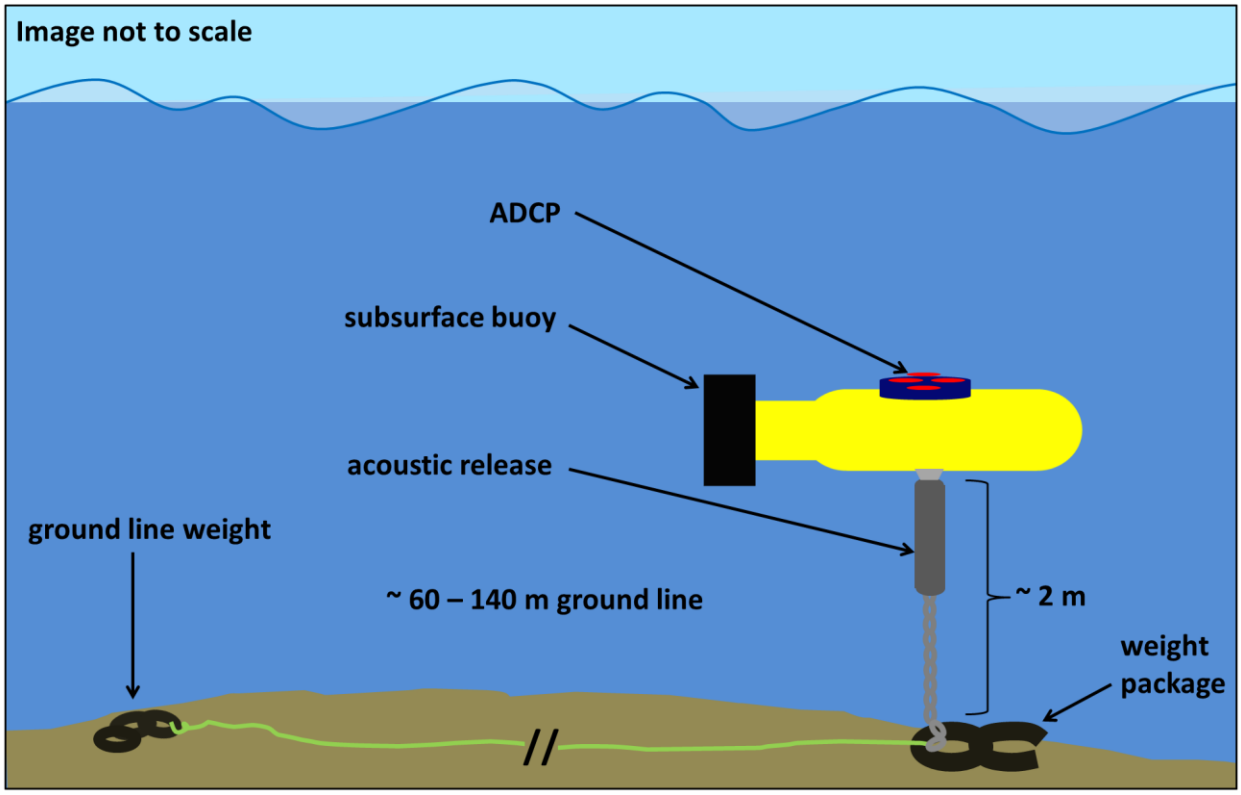

Figure 2. ADCP mooring configuration.

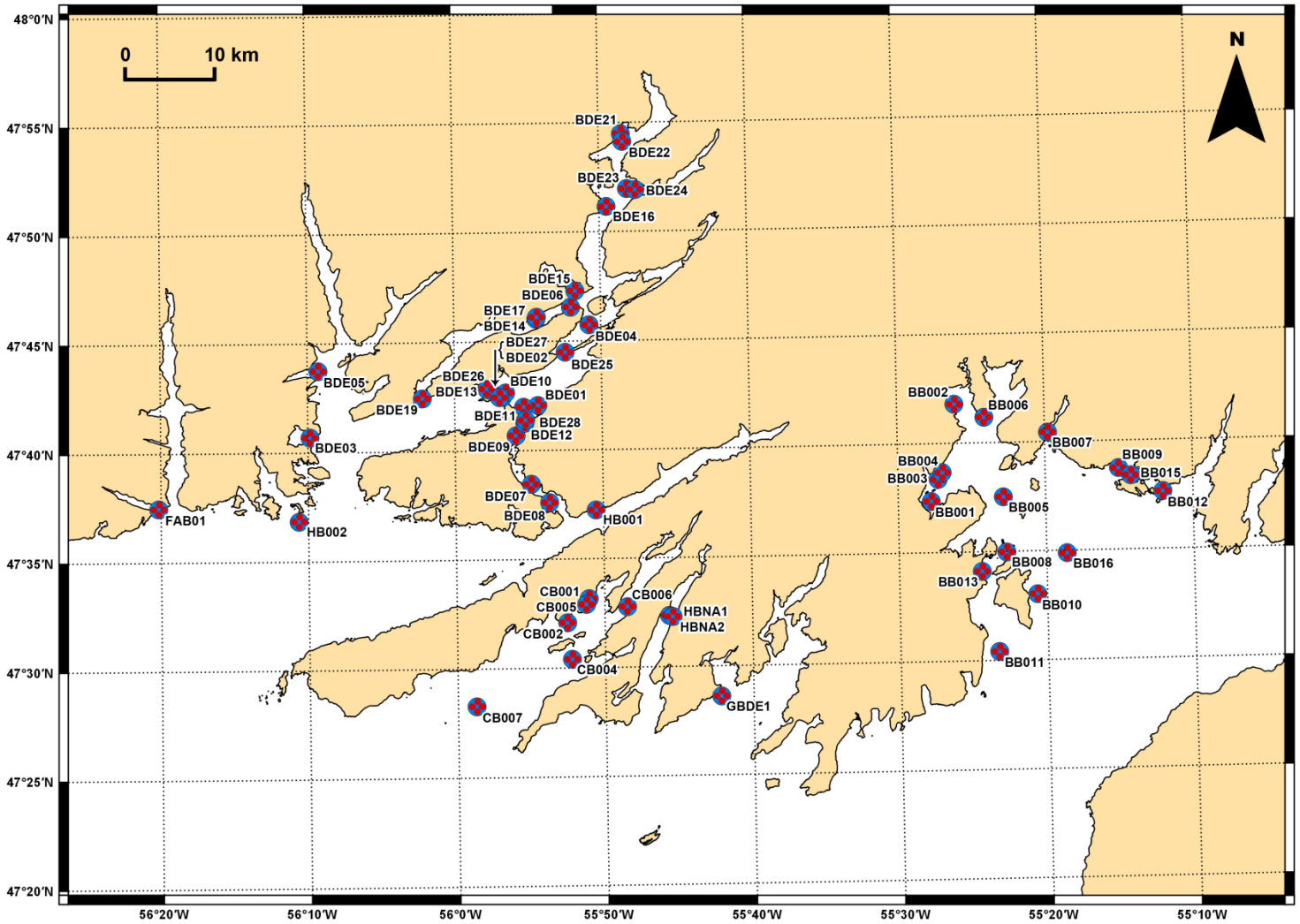

Figure 3. ADCP stations in the Coast of Bay area.

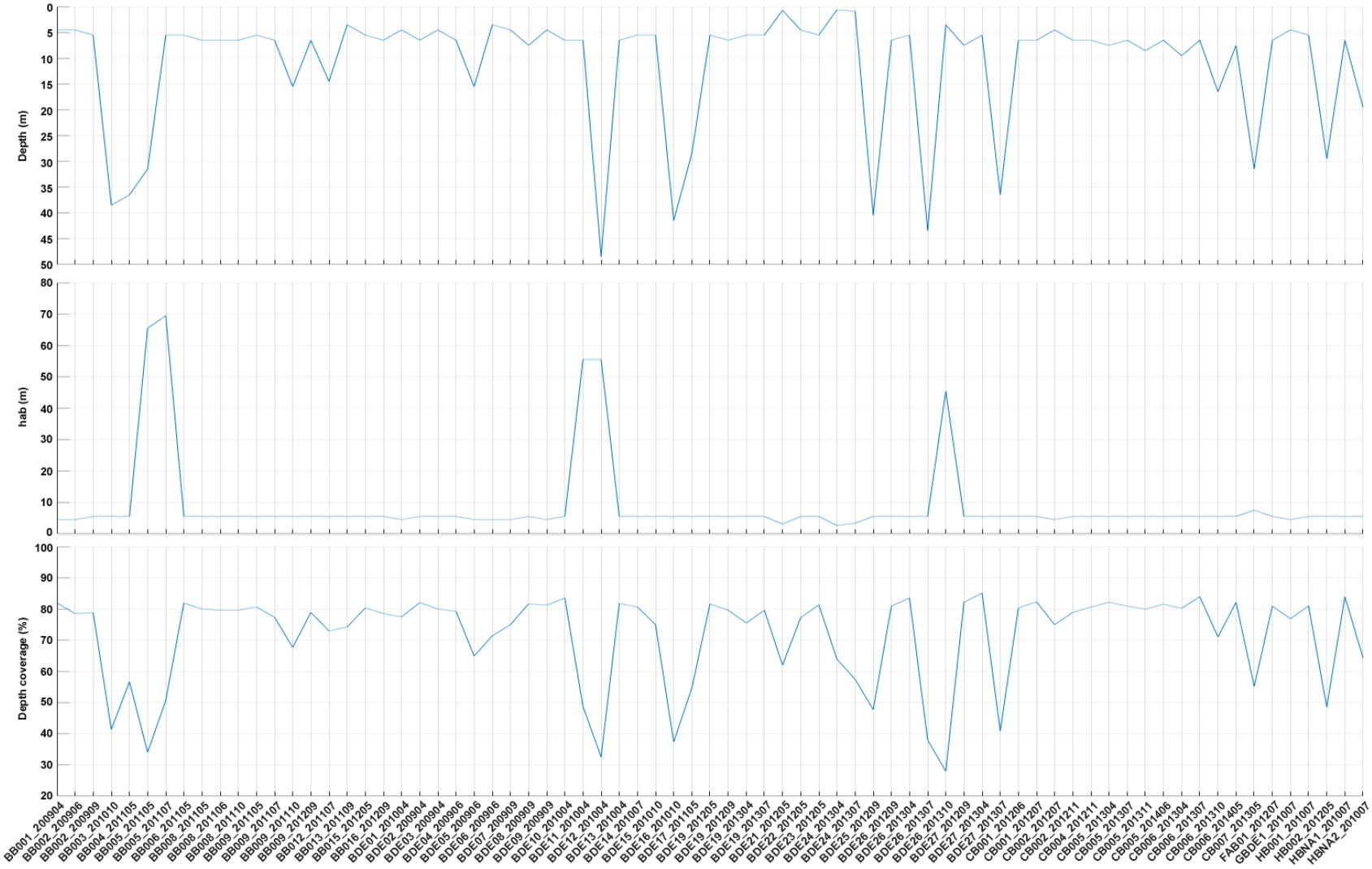

Figure 4. Depth of the first cell measurement (top panel), height above bottom, hab, of the deepest measured cell (mid panel), percentage water column coverage (bottom panel) of the analyzed ocean currents timeseries.

RESULTS

TIMESERIES OF CURRENTS IN THE COAST OF BAYS AREA

Figure 5 illustrates a sample time series of current speed (mag) and direction (dir) in Belle Bay (Station BB008 for the period of 1 Jul. 2011 to 16 Jul. 2011). Sample current roses for near surface layer (7.5 m depth) and near bottom layer (50.5 m depth) are provided in Figure 6. Note the higher speed, above 20 cm/s, found near the surface between 4 and 5 Jul. and between 10 and 13 Jul. which were associated with the passage of a storm (Salcedo-Castro and Ratsimandresy 2013) and the complexity of the vertical structure. Note also the change in the direction of the currents for the upper layer and the layer below. In the upper layer, above approximately 20 m depth, the currents generally show a SSW-NEE dominant direction while in the deeper layer the current direction is more variable with speeds notably lower than those near the surface (Figure 6 for a near surface and a near bottom layer).

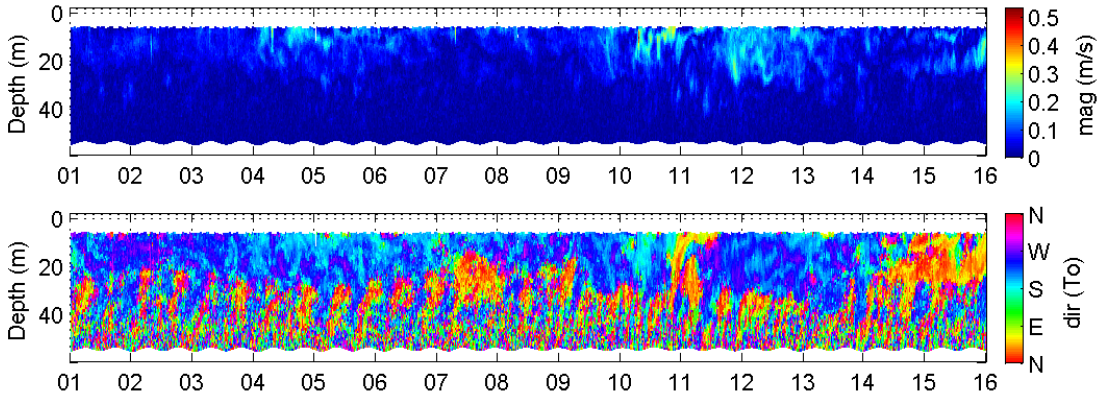

Figure 5. 15 days (1 Jul. 2011 - 16 Jul. 2011) time series of current speed (upper panel) and current direction (lower panel) for station BB008 located in Belle Bay.

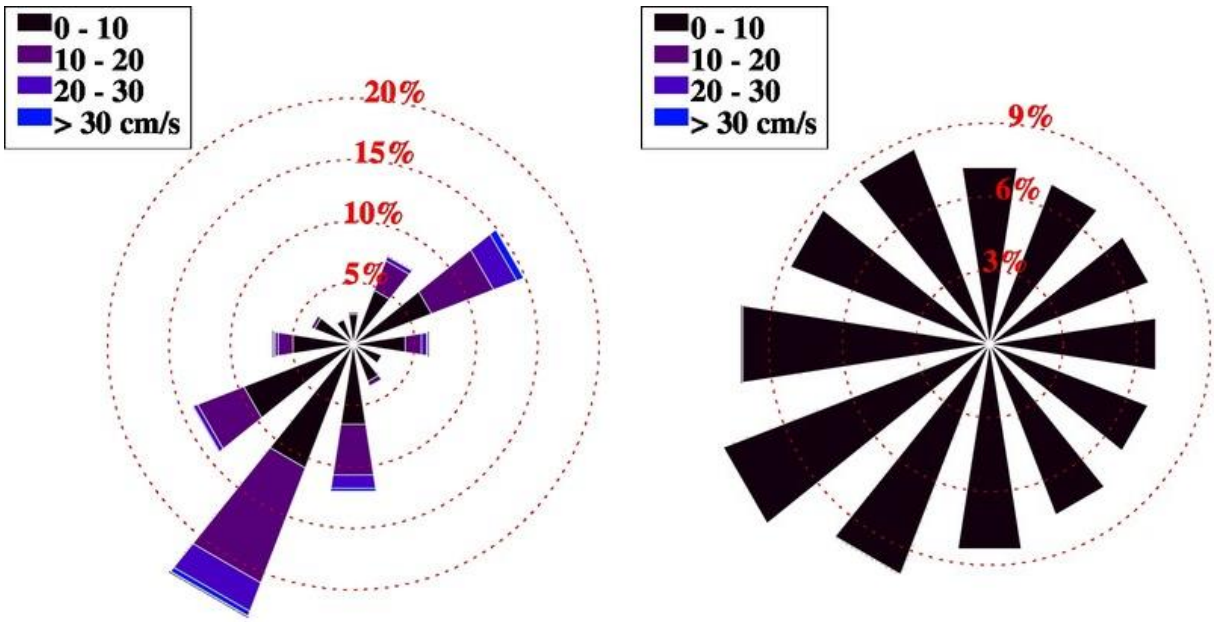

Figure 6. Current roses showing the distribution of current speed and direction at 7.5 m (left panel) and 50.5 m depth (right panel) at station BB008 for the whole measurement period (8 May 2011 to 24 Oct. 2011). Each segment illustrates the direction toward which the currents flow.

ANALYSIS OF CURRENT SPEED

Median current speed

Figure 7 and Figure 8 illustrate the median current speed in the Coast of Bays area for layers above 20 m (upper layer) and below 20 m depth (lower layer), respectively. The median current speed in the upper layer for the whole Coast of Bays area ranges between 2 and 13 cm/s. For the lower layer, the range of median speed is between 1.5 and 13.5 cm/s with this layer generally showing lower speed than the layer above 20 m: the median speed in the upper layer is at least 1.3 times larger than that in the lower layer in 75% of the cases. Differences between locations within the same bay are described below.

Hermitage Bay - Bay D'Espoir

In the upper layer, the median speed ranges between 3 and 13 cm/s with 22 out of 23 stations having median speed below 11 cm/s. The stations with the lowest (BDE07) and the highest (BDE09) median speed were both found within Little Passage. BDE07 is located inside a cove within the passage and is possibly very sheltered from the main current flow. Within BDE, the geographic pattern is that stations in the lower portion of BDE including those in Little Passage tend to show higher values (above 7 cm/s) while those located towards the head and near the mouth of the bay generally showed lower values (below 6 cm/s).

In the lower layer, the range of median values was 2 to 13 cm/s with the lowest value observed at the station near the head of BDE (BDE22) and the highest at the southern mouth of Lampidoes Passage (BDE19). Most of the stations (20 out of 26) showed median speed below 5 cm/s in the lower layer. The rest of the stations (6 out of 26) with values above 5 cm/s were located in the lower portion of BDE and in Little Passage.

When comparing the two layers, the values of the median speed in the upper layer are generally 1-6 cm/s above those in the lower layer with the exception of station BDE19. At this station the upper layer has a median speed of 4 cm/s below that of the lower layer.

Belle Bay

In the upper layer, the median current speed ranges between 2 and 10 cm/s with 8 out of 9 stations having median speed below 10 cm/s. The lowest value was observed within the northwestern head of BB (BB001) and the highest value at a station in the middle of BB (BB016). In comparison to the stations with lower median speed, the stations with higher median speed (above 5 cm/s) tend to be at locations directly exposed to the open water in BB (BB008, BB012, and BB016).

In the lower layer, the median current speed ranges between 2 and 6 cm/s with the lowest value observed at station BB015, on the eastern side of BB, and the highest value at BB016 in the middle of BB. Higher values (above 4 cm/s) are observed at the two stations in the middle of BB (BB005 and BB016).

Comparison between the two layers shows that the median current speeds in the upper layer are generally above those in the lower one with differences up to 5 cm/s.

Connaigre Peninsula

In the upper layer of CP, the range of the median current speed is between 3 and 7 cm/s with two stations (CB004 and GBDE1) showing values above 6 cm/s and the rest (5 stations) showing values below 6 cm/s. The two stations with higher median speeds are located in the area more exposed to the open ocean.

In the lower layer, the range is between 2 and 5 cm/s. Two stations in CB show higher values (above ~5 cm/s for CB004 and CB007, located towards the open ocean) and the rest (7 stations) show values below 4 cm/s.

When comparing the two layers, the values in the upper layer are above those in the lower layer by 1 to 2 cm/s of differences.

Maximum recorded current speed

Figure 9 and Figure 10 present the maximum current speed recorded at each station for the upper and the lower layers, respectively.

In the upper layer, the highest maximum current speed (90 cm/s) was recorded at the station BDE19 at the southwestern mouth of Lampidoes Passage and the lowest maximum speed at BB013 (~22 cm/s), a station northwest of Chapel Island.

In the lower layer, the highest maximum current speed was 90 cm/s also recorded at station BDE19 in BDE. In this layer, the lowest maximum current speed (~14 cm/s) was observed at station BB001 in a sheltered cove of BB.

Comparison of the maximum recorded speed between the upper and the lower layers (Appendix 3) shows that 89% of the stations with data in both layers had experienced stronger current speed in the upper layer than in the lower layer (with differences between 4 and 40 cm/s); the rest of the stations (11 %) showed maximum current speed of similar range (differences less than 4 cm/s between the two layers). No geographic pattern was found for the location of these stations.

Spread of the current speed

Figures 11, 12, 13, 14, 15, and 16 summarize the centre and spread of current speed in the upper and lower layer for HB-BDE, BB, and CP, respectively. Statistics were not computed for HBNA2 upper layer, in CP, as data were only available between 19 and 20 m depth while statistics for BDE05 upper layer in HB-BDE were carried out with data from 15-20 m depth. The

figures show that the stations with low (high) median current speed also experienced low(high) IQR and upper fence values.

For each region, the comparison between the two layers shows that the median speed, the IQR, and the upper fence values are higher in the upper layer than in the lower one with the exception of station BDE19 in BDE.

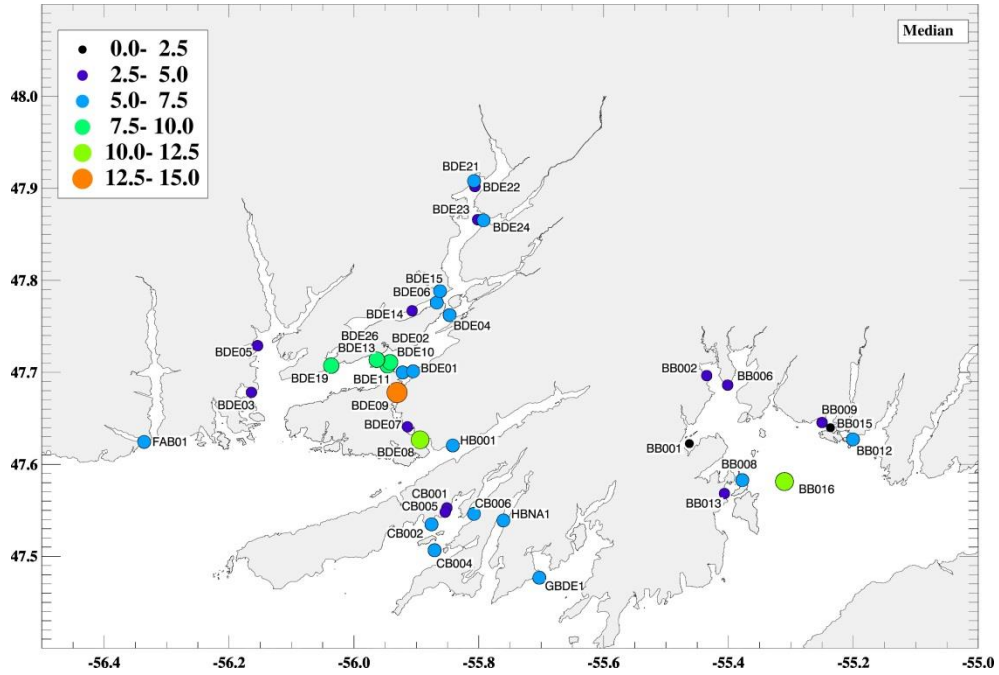

Figure 7. Median current speed [cm/s] in the upper layer for the Coast of Bays region.

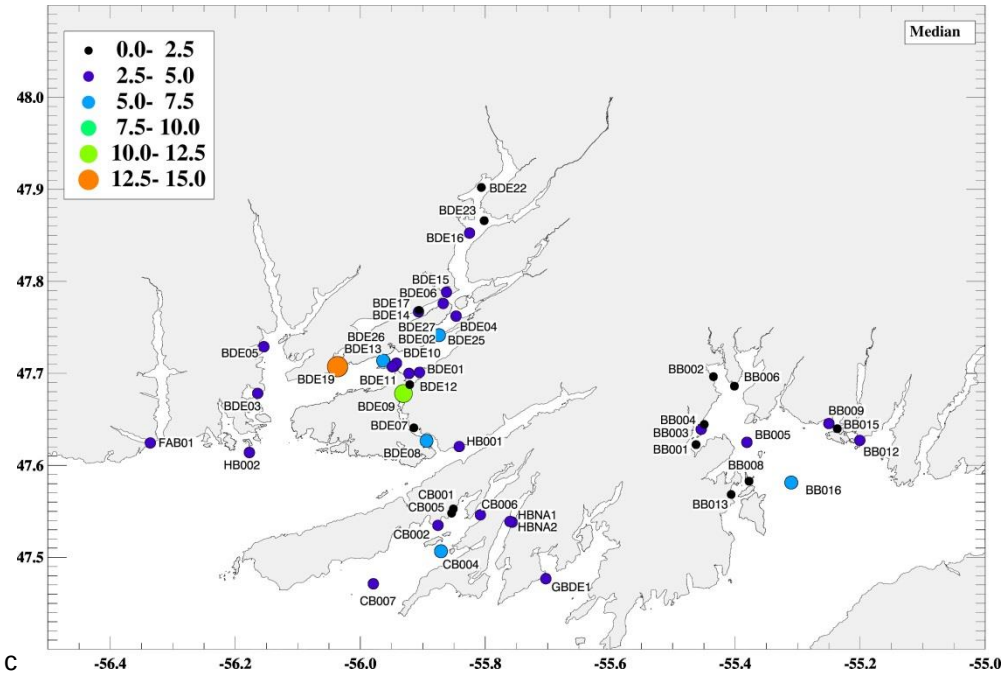

Figure 8. Median current speed [cm/s] in the lower layer for the Coast of Bays region.

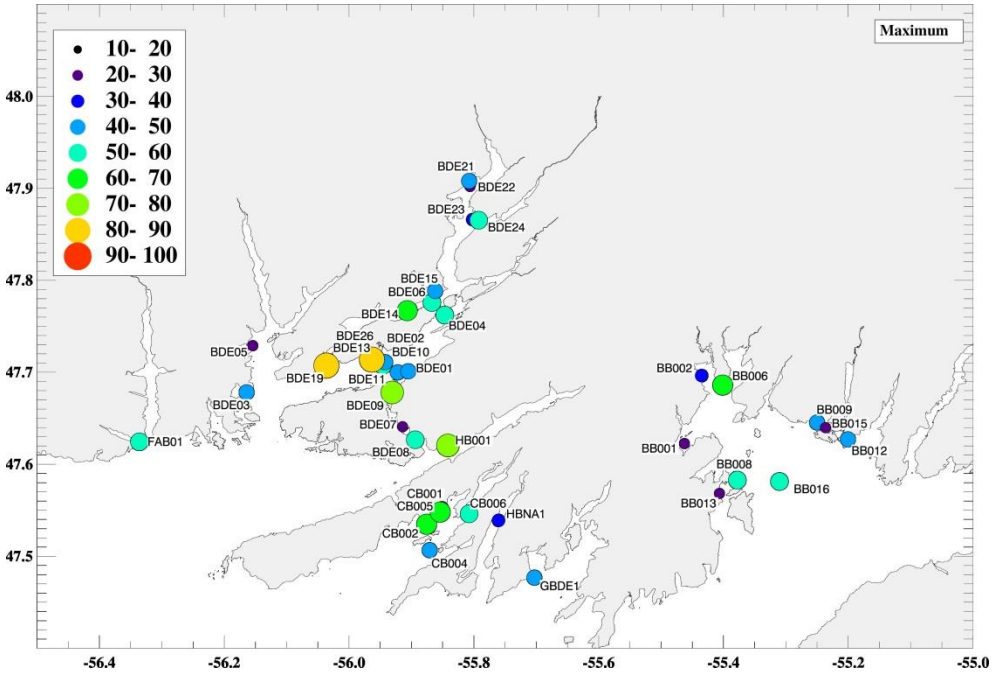

Figure 9. Maximum current speed [cm/s] recorded in the upper layer.

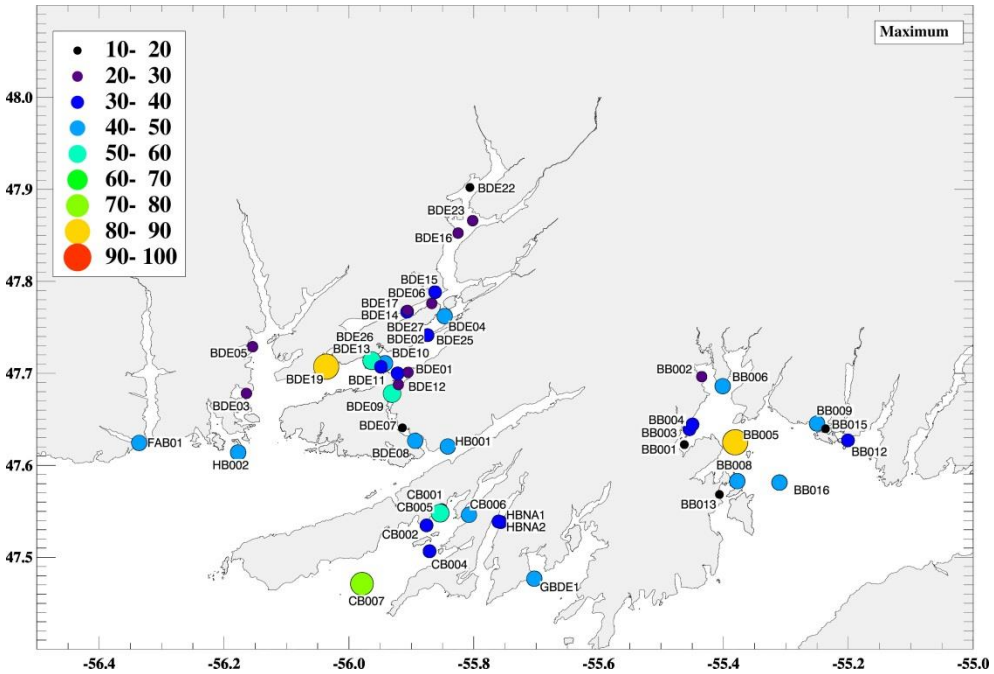

Figure 10. Maximum current speed [cm/s] recorded in the lower layer.

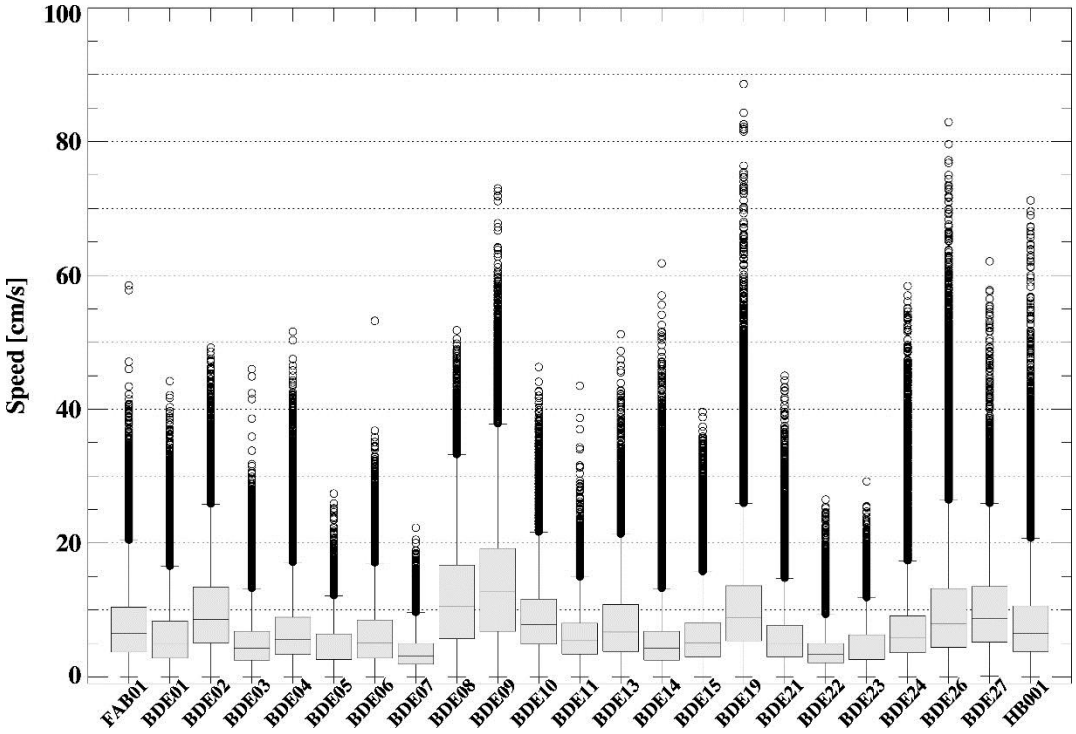

Figure 11. Box and whisker plot of the current speed in the upper layer (above 20m) for data measured in HB-BDE. The plot provides information on median and interquartile range (IQR) of data, current speeds above the upper fence (values above 1.5xIQR from the third quartile) are represented with open circles.

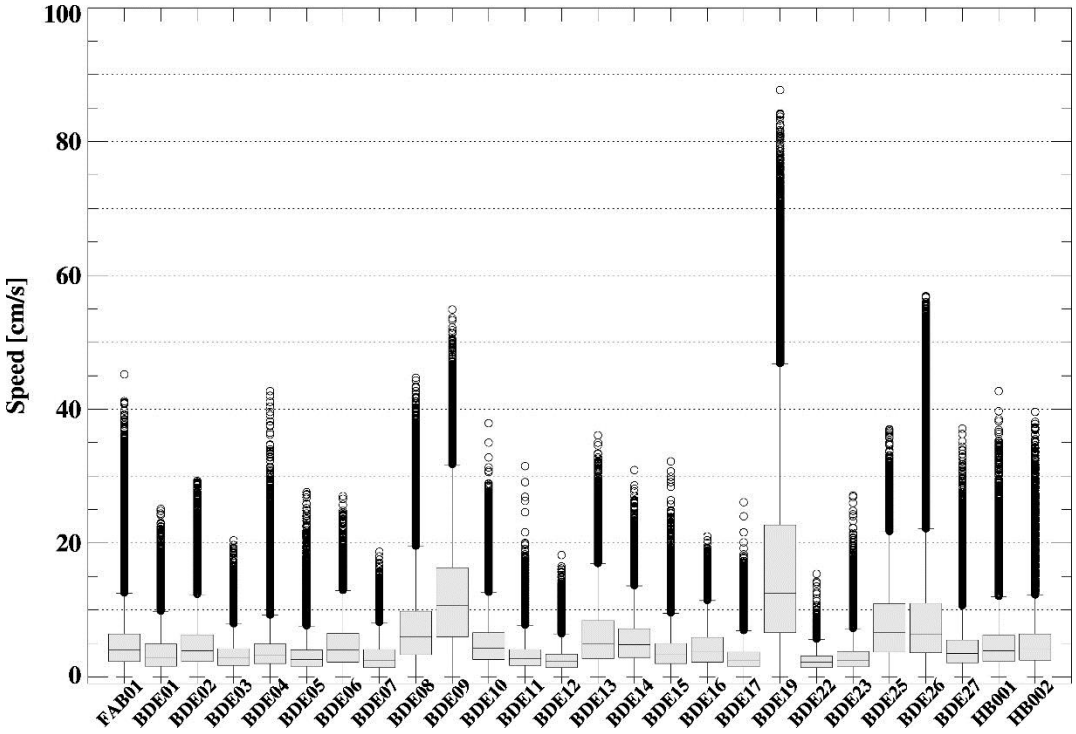

Figure 12. Box and whisker plot of the current speed in the lower layer (below 20m) for data measured in HB-BDE (analogous to Figure 11).

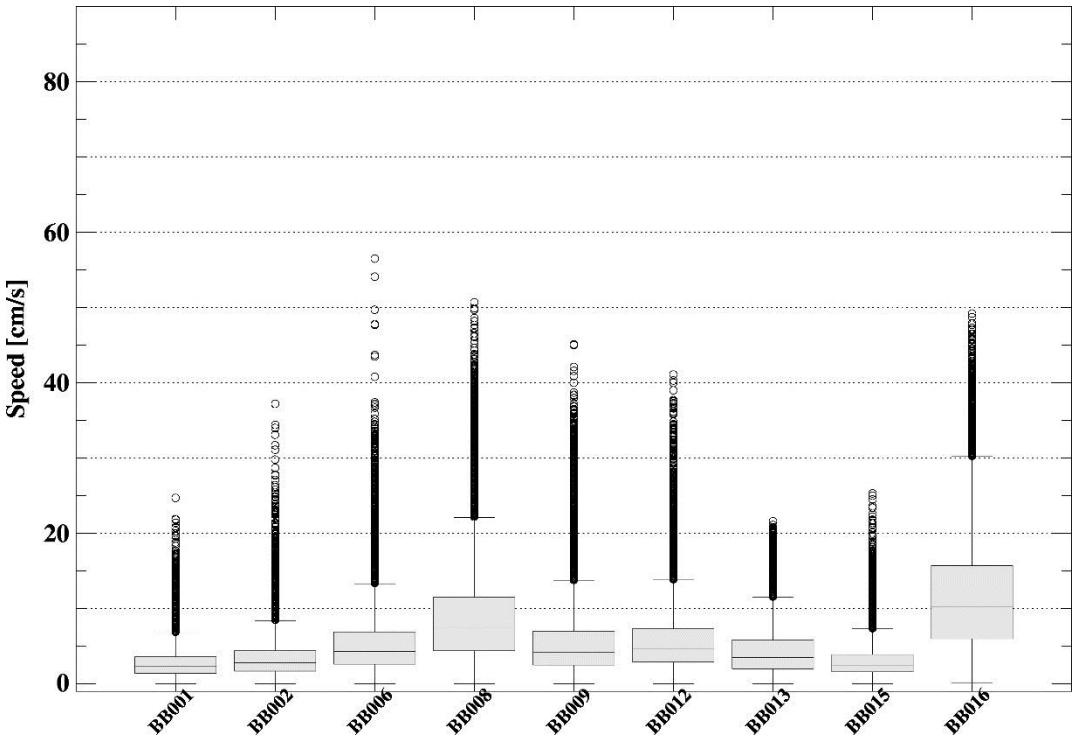

Figure 13. Box and whisker plot of the current speed in the upper layer (above 20m) for data measured in BB (analogous to Figure 11).

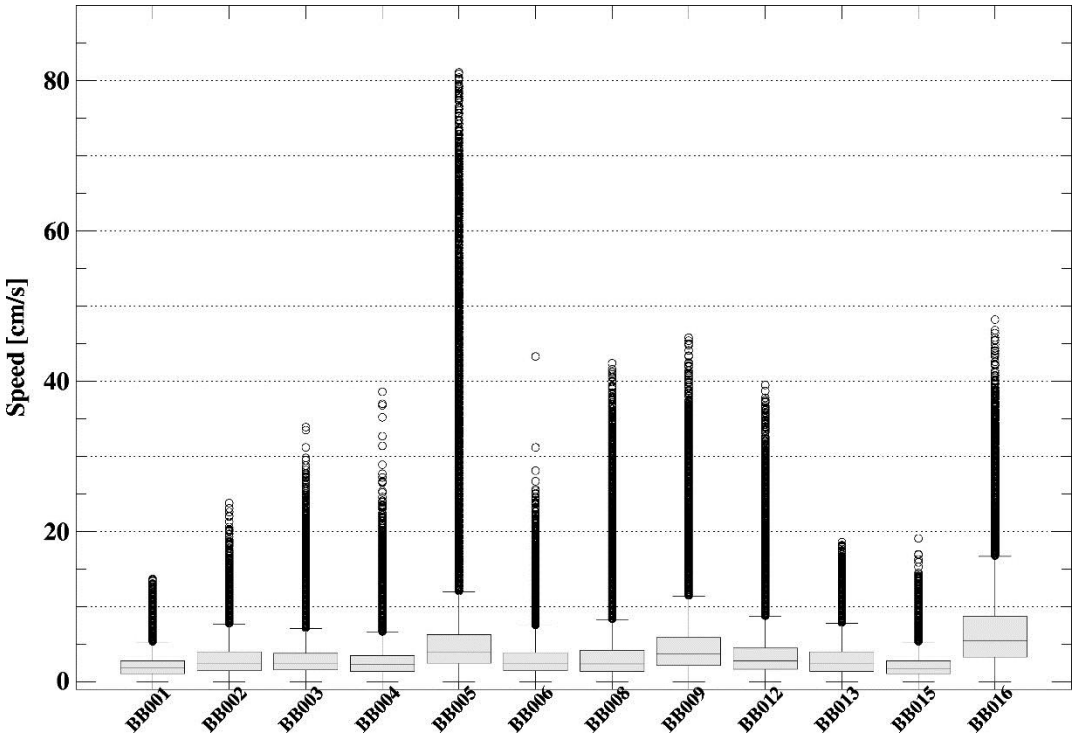

Figure 14. Box and whisker plot of the current speed in the lower layer (below 20m) for data measured in BB (analogous to Figure 11).

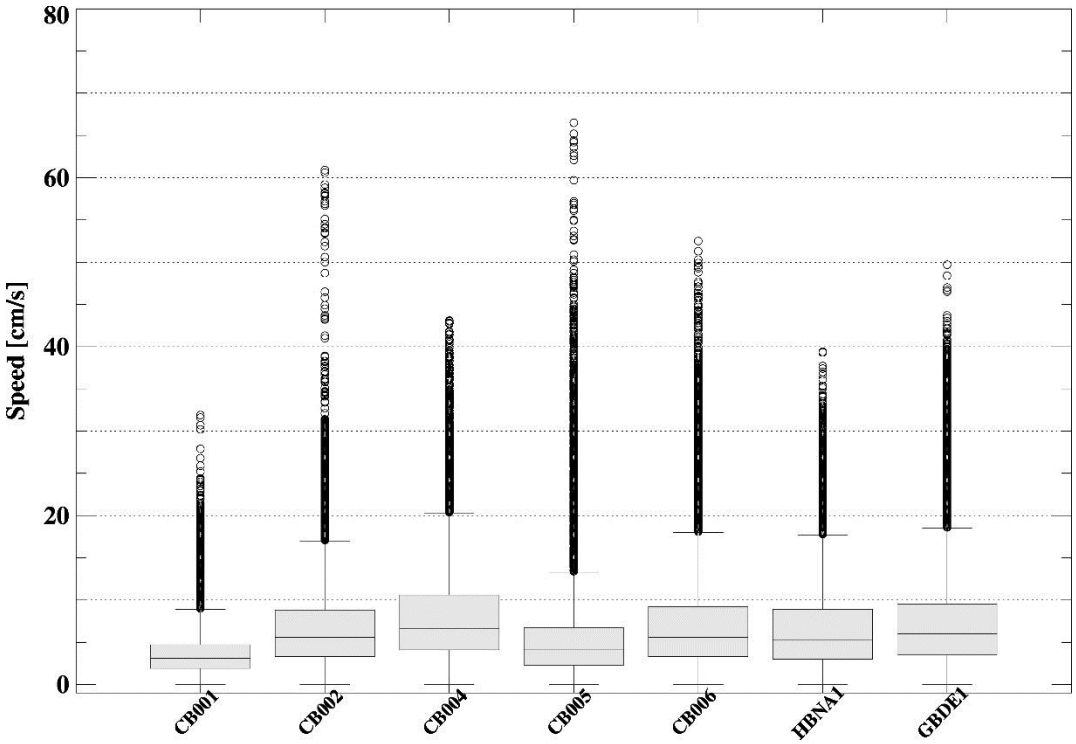

Figure 15. Box and whisker plot of the current speed in the upper layer (above 20m) for data measured in CP (analogous to Figure 11).

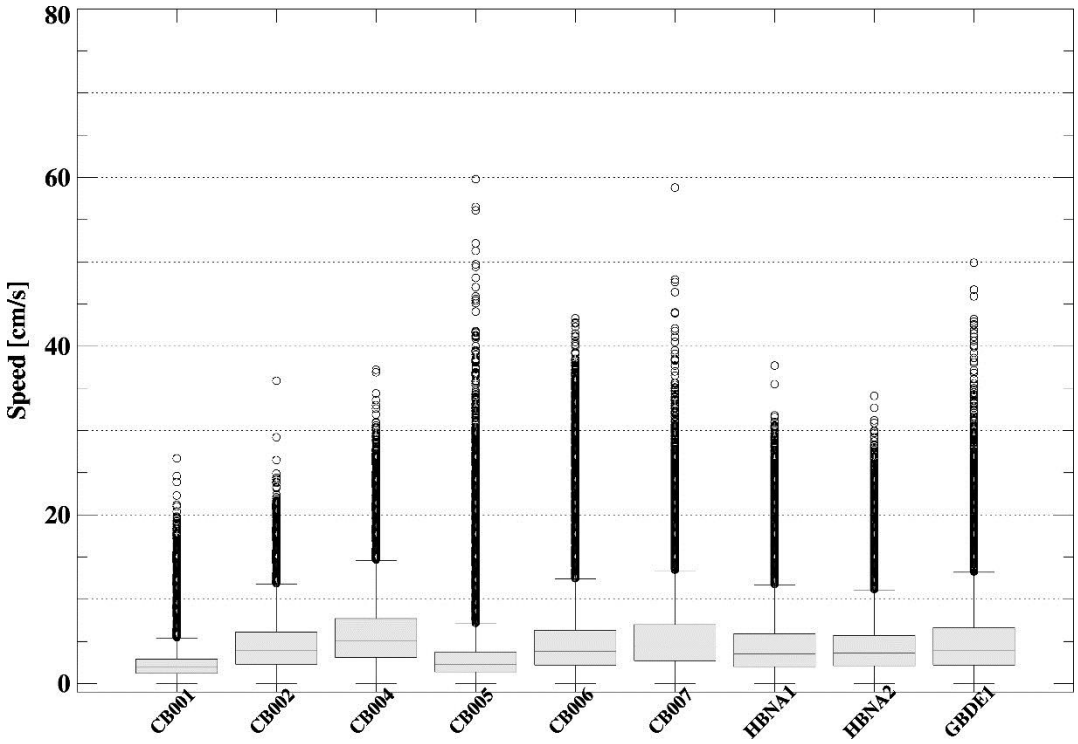

Figure 16. Box and whisker plot of the current speed in the lower layer (below 20m) for data measured in CP (analogous to Figure 11).

Temporal variability

Maps showing the median current speed for the upper layer for different seasons are presented (Figure 17). Note that winter map is not provided as only few stations were visited in winter. Despite the fact that stations were not always revisited, one can observe an increase in the median currents in fall as shown in Little Passage (BDE) and on the western side of BB. As for the recorded maximum currents (Figure 18), most stations showed upper layer maximum current speed above 40 cm/s without any specific seasonal nor spatial pattern. This lack of pattern can be attributed to the fact that strong currents which are generally associated with strong atmospheric events (Salcedo-Castro and Ratsimandresy 2013) can occur in any season of the year as the whole region is prone to strong winds all year long (Donnet et al. 2018a). In the lower layer, some increase in the median current speed (Figure 19) in fall is also observed. Maximum current speed above 40 cm/s was also recorded at various stations for different seasons. A slightly higher maximum current speed in fall season can be observed in BB and at sill locations in Little Passage (Lower BDE, Figure 20).

Few stations have been revisited for longer than a 4 month period (Appendices 1 and 2). Current speed data from these stations were used to investigate the monthly variability. Data have been grouped on a monthly basis and monthly variability was assessed. Figure 21 illustrates examples of monthly statistics of current speed in the upper layer for stations in HB-BDE (BDE19), in BB (BB008), and in CP (CB006). The figure shows monthly variation of the median current speed with lower speed late spring/summer and higher speed in fall. The change between the lowest and highest calculated monthly median speeds was 45% for BDE19, 47% for BB008, 53% for CB006. Maximum current speed shows the highest variation from month to month with higher maximum speed occurring generally in summer or fall and lowest in winter or early spring (a variation between the lowest and the highest values of 116% for BDE19, 78% for BB008, 118% for CB006).

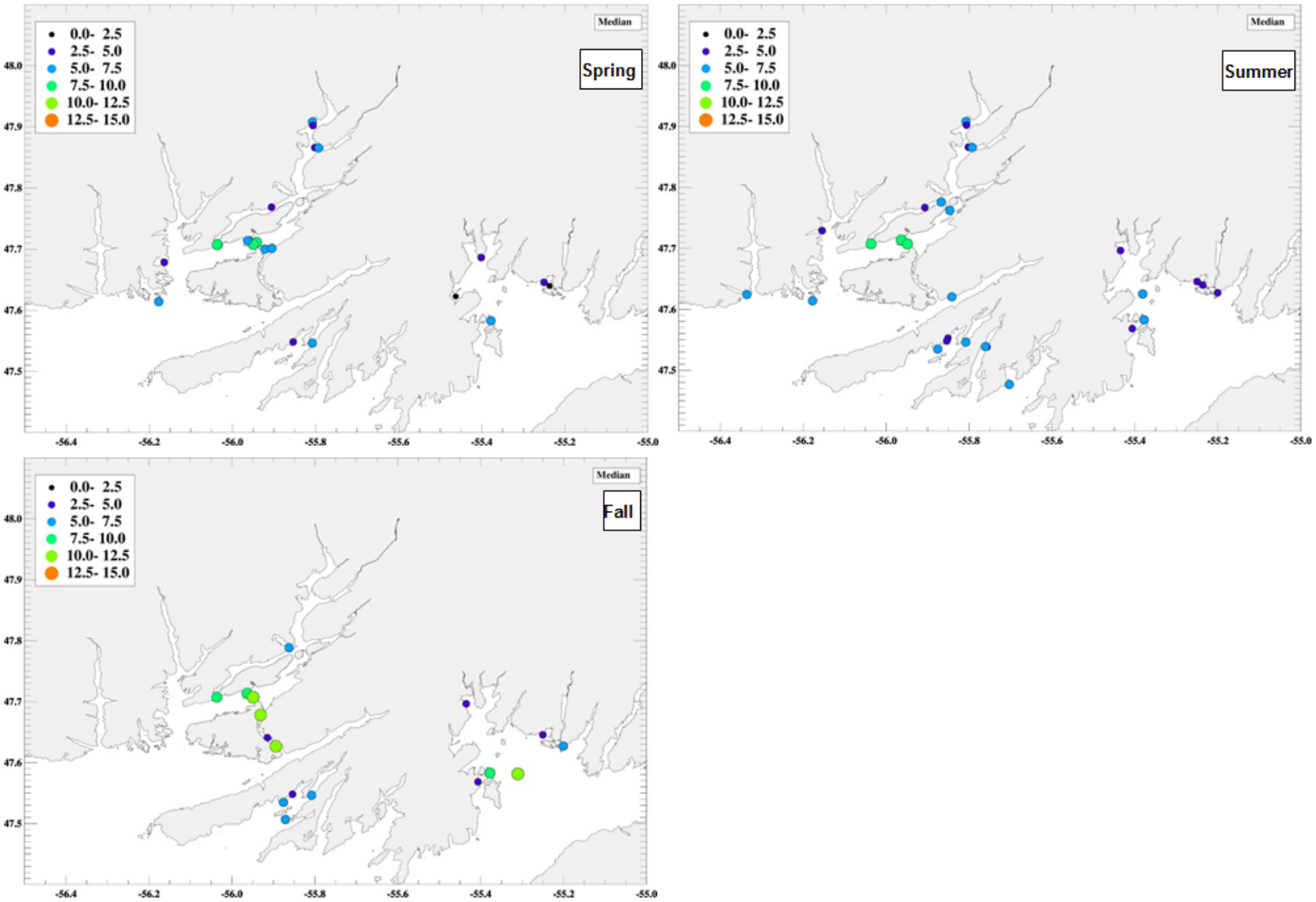

Figure 17. Seasonal variability of the median currents (cm/s) in the upper layer for Spring, Summer, and Fall.

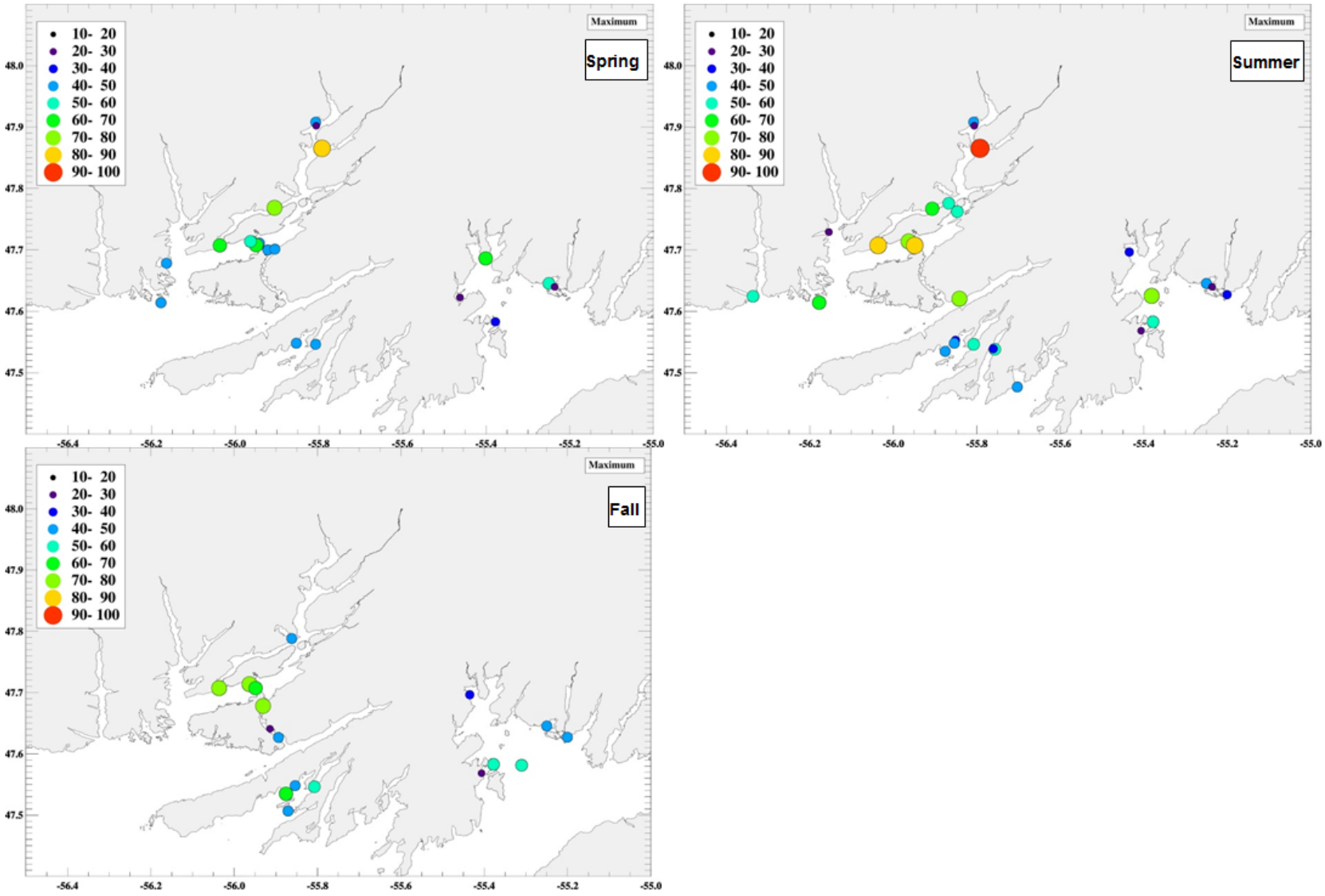

Figure 18. Seasonal variability of the maximum current speed (cm/s) in the upper layer for Spring, Summer, and Fall.

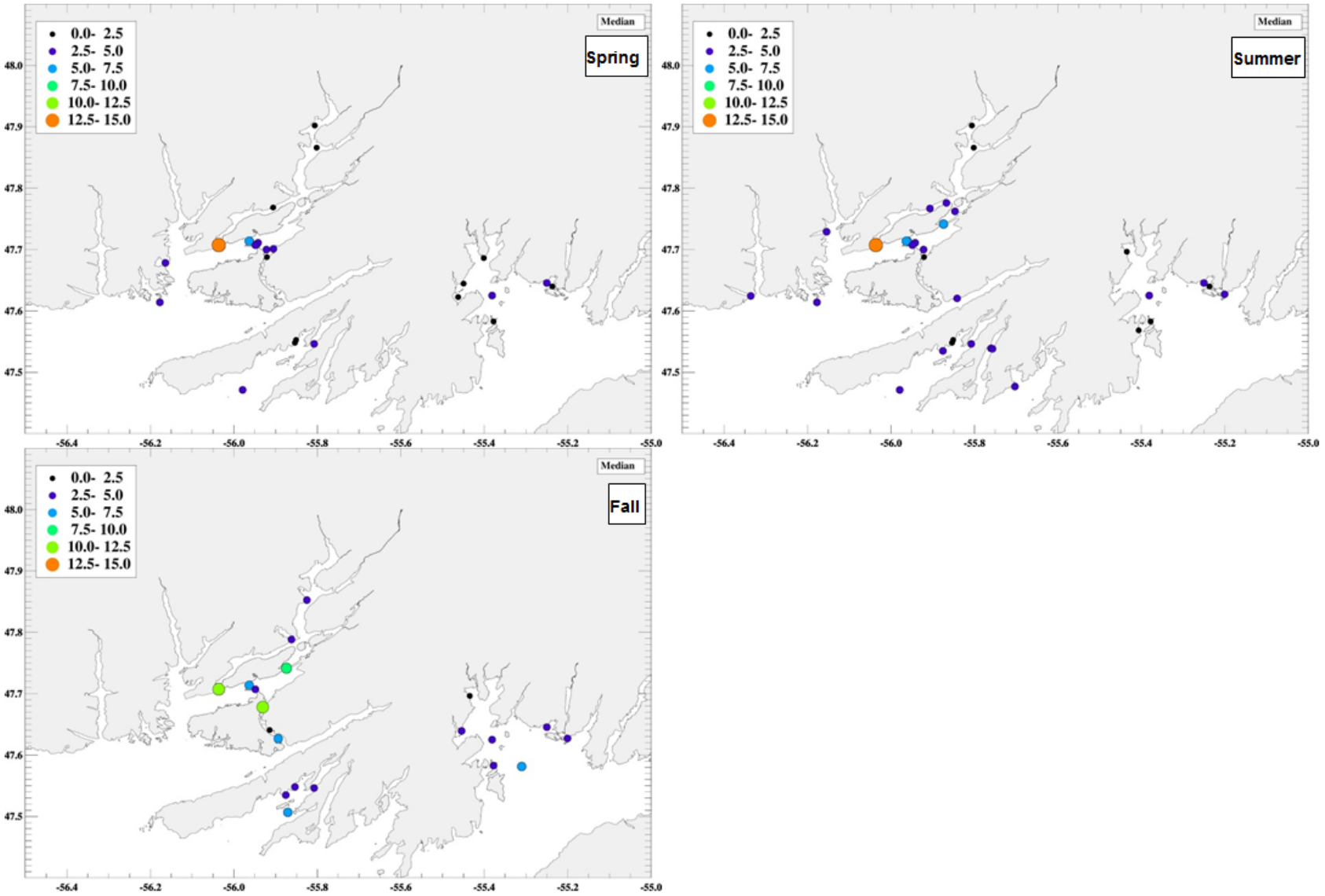

Figure 19. Seasonal variability of the median currents (cm/s) in the lower layer for Spring, Summer, and Fall.

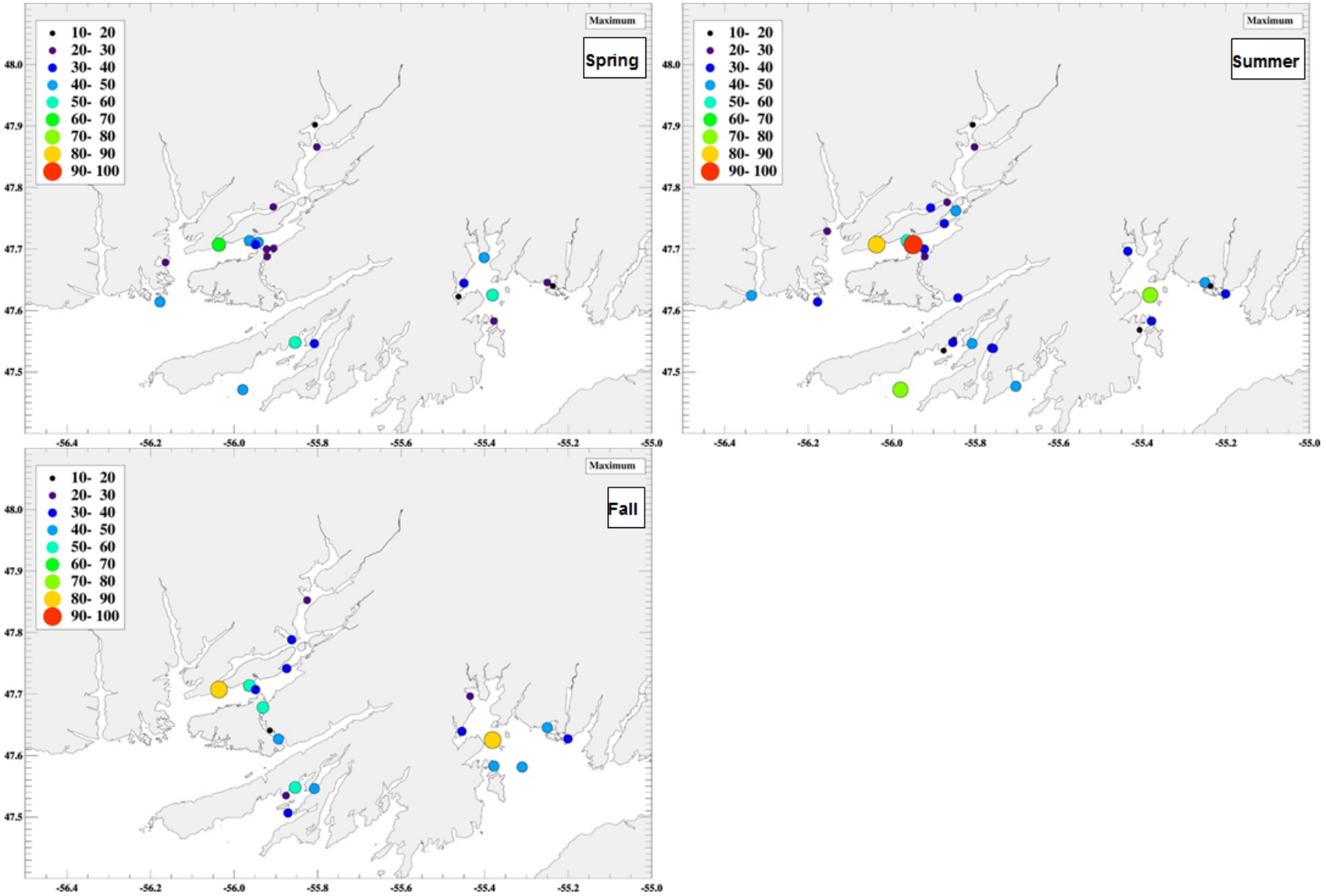

Figure 20. Seasonal variability of the maximum current speed (cm/s) in the lower layer for Spring, Summer, and Fall.

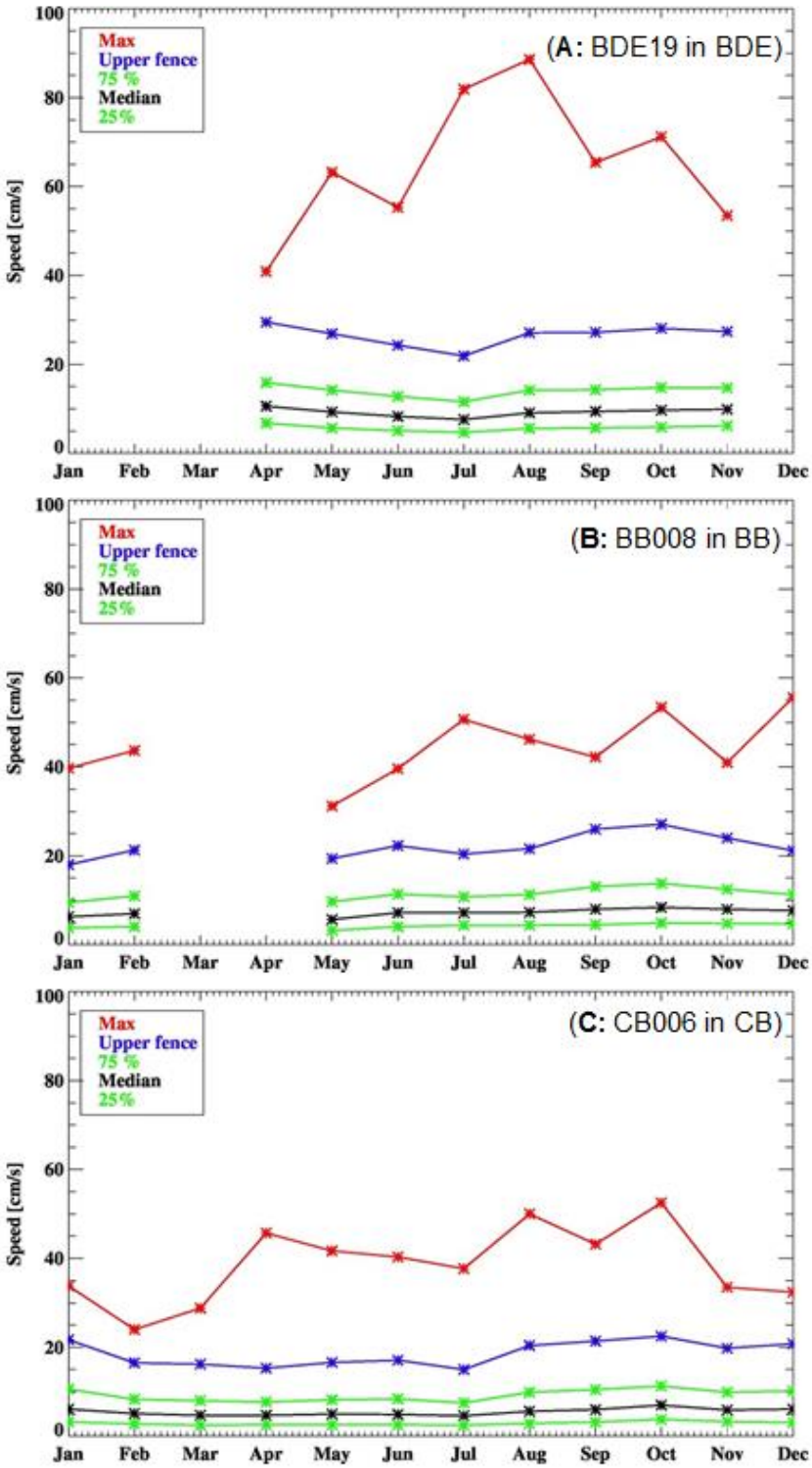

Figure 21. Example of monthly variability of current speed in the upper layer for stations (A) BDE19 in BDE, (B) BB008 in BB, and (C) CB006 in CB. 25%, median, and 75% represent the 25, 50, and 75 percentiles, upper fence is the value as described in the methodology on summary statistics and Max is the maximum recorded current speed.

CURRENT VELOCITY ANALYSIS

The following set of figures (Figure 22 to Figure 27) illustrates the mean and maximum currents at each station. In contrast to the previous analysis where the calculation was performed over a range of depth (one for upper layer and one for lower layer) and due to rapid changes in current direction occurring within the water column at many of the stations, the mean current is computed at each available depth. The description of the main key points for each region is presented below.

Hermitage Bay – Bay D'Espoir

Figure 22 shows the mean currents in the upper and lower layers for HB-BDE with the color of the vector representing different depths. The magnitude of the mean current velocity is about half the median speed computed in the previous analysis; an indication of temporal changes in the direction of the currents. The circulation is complex as described below for measurements made from the mouth of BDE toward the head (see Figure 1 for island and passage names):

- In the lower portion of BDE, the general pattern is a circulation going out of the bay.
- However, measurements carried out in the little Passage generally show mean currents going into the bay below 5 m depth except at BDE07 where the direction of the mean currents below ~10 m depth is towards outer bay.
- Observed mean currents at stations near the head of the bay tend to be smaller and show opposite directions between surface layers (~above 5 to 10 m) and the layers below. This circulation with opposite mean directions at different depths might be the result of complex estuarine circulation, potentially affected by varying prevailing winds, and the presence of eddies.
- Mean currents at the southwestern mouth of Lampidoes Passage flow out of the bay in the upper part of the lower layer and slowly turn counterclockwise towards the sea-bottom.
- At the southern part of Little Passage, the whole lower layer shows mean currents going into the bay except at BDE07.
- Mean currents in the lower layer tend to be lower towards the head of the bay.

For the maximum currents recorded at each depth (Figure 23), it is worth noting the change of scale of the vector. The strongest currents recorded in the area have speeds in the range of 50 cm/s (10 times larger than the mean current). Here also, direction of the currents changes depending on depth and station. Observed main features to note are:

- The strongest recorded currents at the mouth of Lampidoes Passage, station BDE19, were mainly directed to the south (i.e., out of the bay) in the upper ~50 m depth and then to the north (i.e., into the bay) in the layer below,
- The strongest currents recorded north of Isle Galet were directed out of the bay within the upper layer, down to about 15 m, then into the bay down to about 25-30 m and then out of the bay again below 30 m depth,
- The strongest recorded currents in Little Passage (BDE09 and BDE08) and toward the head of HB (HB001) were going into the bay, at all depths in the upper layer except at BDE07 that showed reversal around 10 m,
- The strongest recorded currents were directed out of the bay in the lower layer of Upper BDE.

- At some sites the strongest currents at different depths can equally have in or out of the bay direction (e.g., HB001, HB002, BDE03) or any direction (e.g. BDE14 and BDE17).

Interpretation of these observations is difficult due to the fact that the vectors represent a one-time measurement and maximum currents at different depths may represent different times and events.

Belle Bay

The mean currents in BB are much lower than those in HB-BDE in the upper and in the lower layer (Figure 24). The main features to note are:

- The very low mean currents in Cinq Island Bay in the whole water column.
- The southward mean currents north of Chapel Island (for the whole water column).
- The westward to northeast-ward currents in the middle of BB with the direction turning clockwise as the layer gets deeper. At depth the currents are consistent with the bathymetry of the site, indicating topographic steering.
- North of Rencontre Island, the mean currents in the upper 20 m show inshore direction (eastward) and offshore (westward) at depths (roughly below 40 m). East of the island (BB012), the mean currents also show inshore direction (westward) in the upper ~35 m and start to veer to the southwest at depths.

For the maximum currents observed in BB (Figure 25), strong currents (in the range of 50 cm/s) were recorded in the upper as well as the lower layers. Weaker strongest currents (less than ~30 cm /s) were observed in the Cinq Islands Bay. In the other part of the bay, the direction of the observed strongest currents shows some degree of layering where the strongest currents near the surface went to one direction and those at depths went to other directions. For instance, Station BB009, in the northeast, showed strongest currents going inshore in the upper ~35 m and going offshore at depths; for Station BB008, north of Chapel Island, the strongest currents above and below ~10 m depth went in the northeast (offshore) and the west-southwest, respectively; for Station BB005, in the channel near Dog Island, the change of direction occurred around 60 m depth.

Connaigre Peninsula

Figure 26 illustrates the mean currents in CP region for upper and lower layers. Overall, the mean currents in the whole water column are of the same order of magnitude as or slightly larger than those in BB. The main features are:

- The mean currents within Connaigre Bay are generally going out of the bay (upper and lower layers) except near the head (CB006 and the deeper part of CB004).
- Mean currents in Northeast Arm show direction towards the head in the upper 50 m depth. From 50 m to the bottom the mean currents start veering towards the mouth of the bay.

For the strongest currents recorded in CP (Figure 27), the main features are:

- For stations on the eastern side of Connaigre Bay, the recorded strongest currents in the upper 20 m depth show a tendency to go towards one direction while maximum currents at deeper depths are more variable in direction. On the north-western side of the bay, the direction of the strongest currents is more variable over the whole depth.

- In Northeast Arm, the strongest recorded currents were directed towards the head of the arm in the layer (5 to ~30 m depth) while at deeper depths (roughly below 30 m) the direction of recorded strongest currents were out of the arm.
- On the western side of GBDE the strongest currents near the surface (in the upper ~10 m) were recorded going into the bay while below that depth the strongest currents went out of the bay.

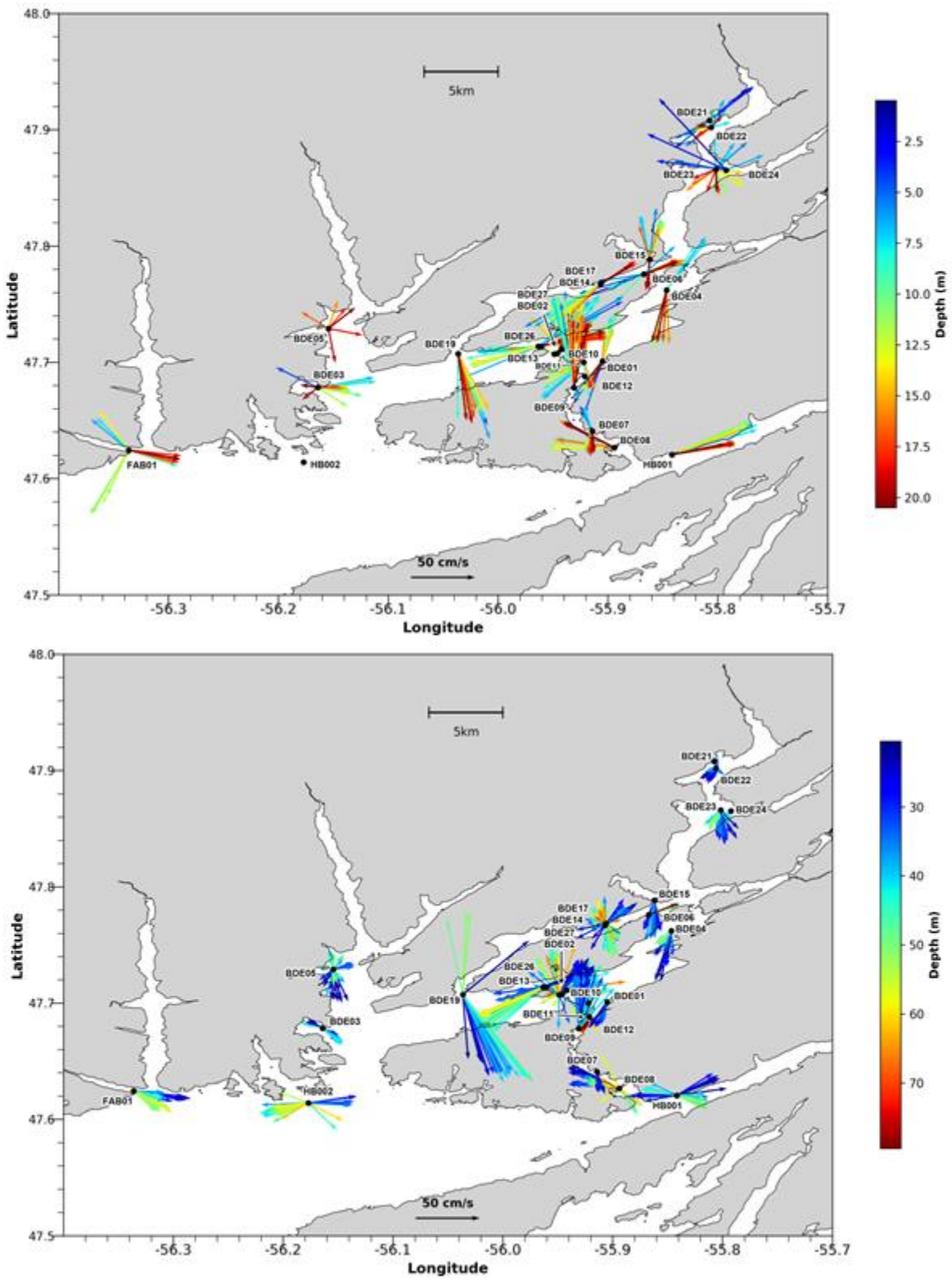

Figure 22. Mean currents in the upper layer (top panel) and lower layer (bottom panel) for HB-BDE.

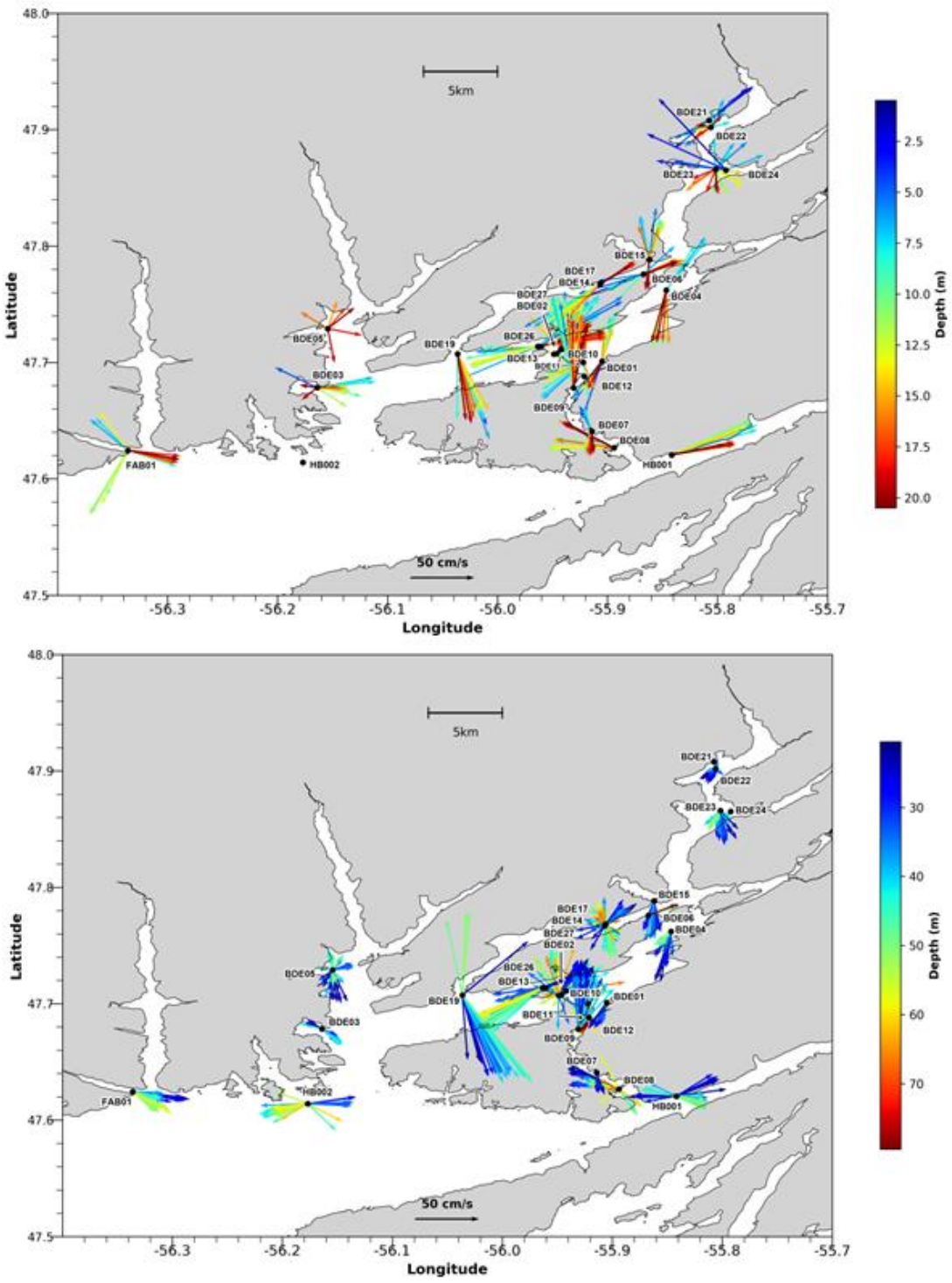

Figure 23. Maximum currents recorded in HB-BDE for the upper layer (top panel) and for the lower layer (bottom panel).

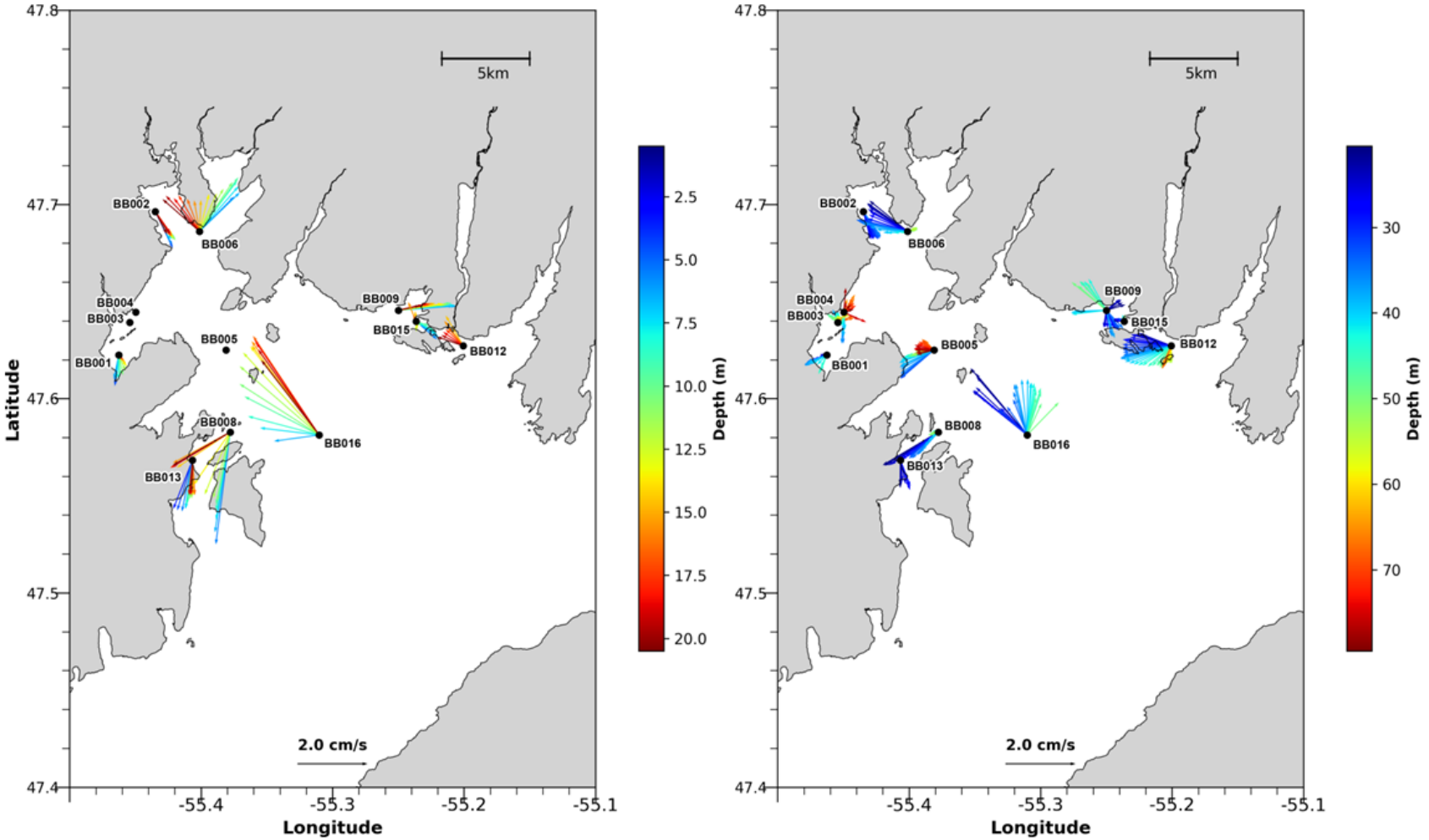

Figure 24. Mean currents in the upper layer (left panel) and lower layer (right panel) for BB region. Dots any current arrow means data were not available. Note the change of scale for BB currents.

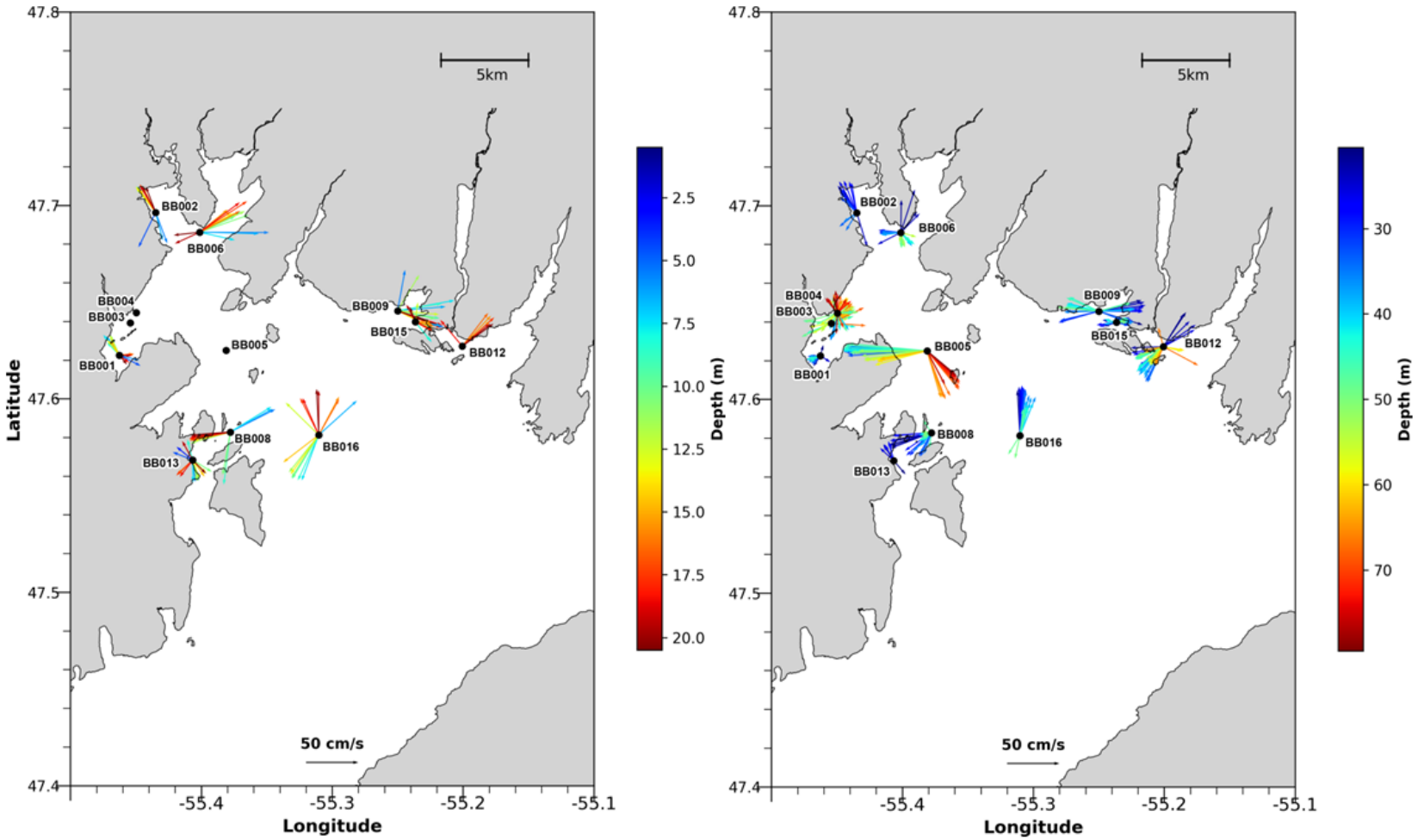

Figure 25. Maximum currents recorded in Belle Bay for the upper layer (left panel) and for the lower layer (right panel).

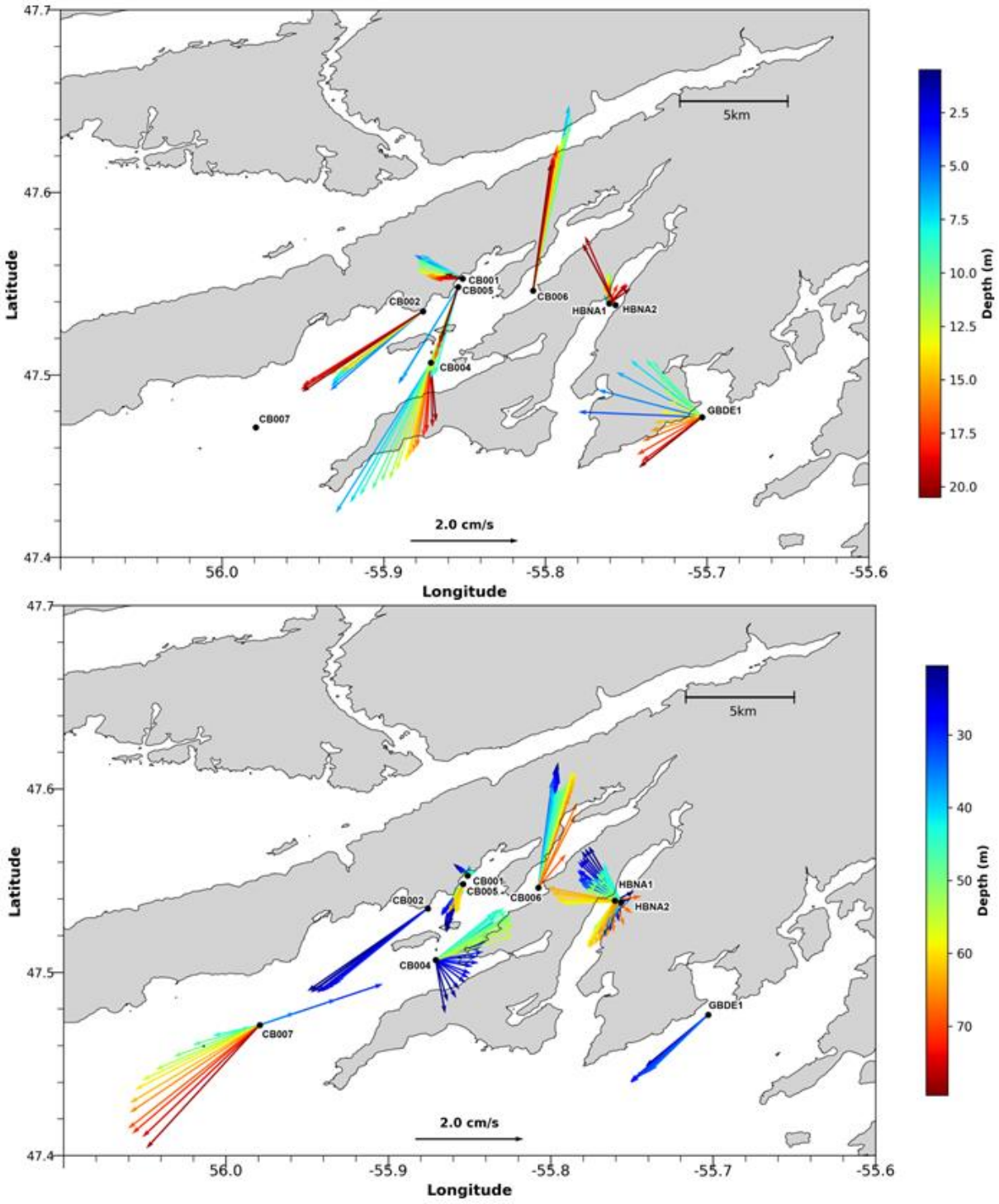

Figure 26. Mean currents in the upper layer (top panel) and lower layer (bottom panel) for CP region.

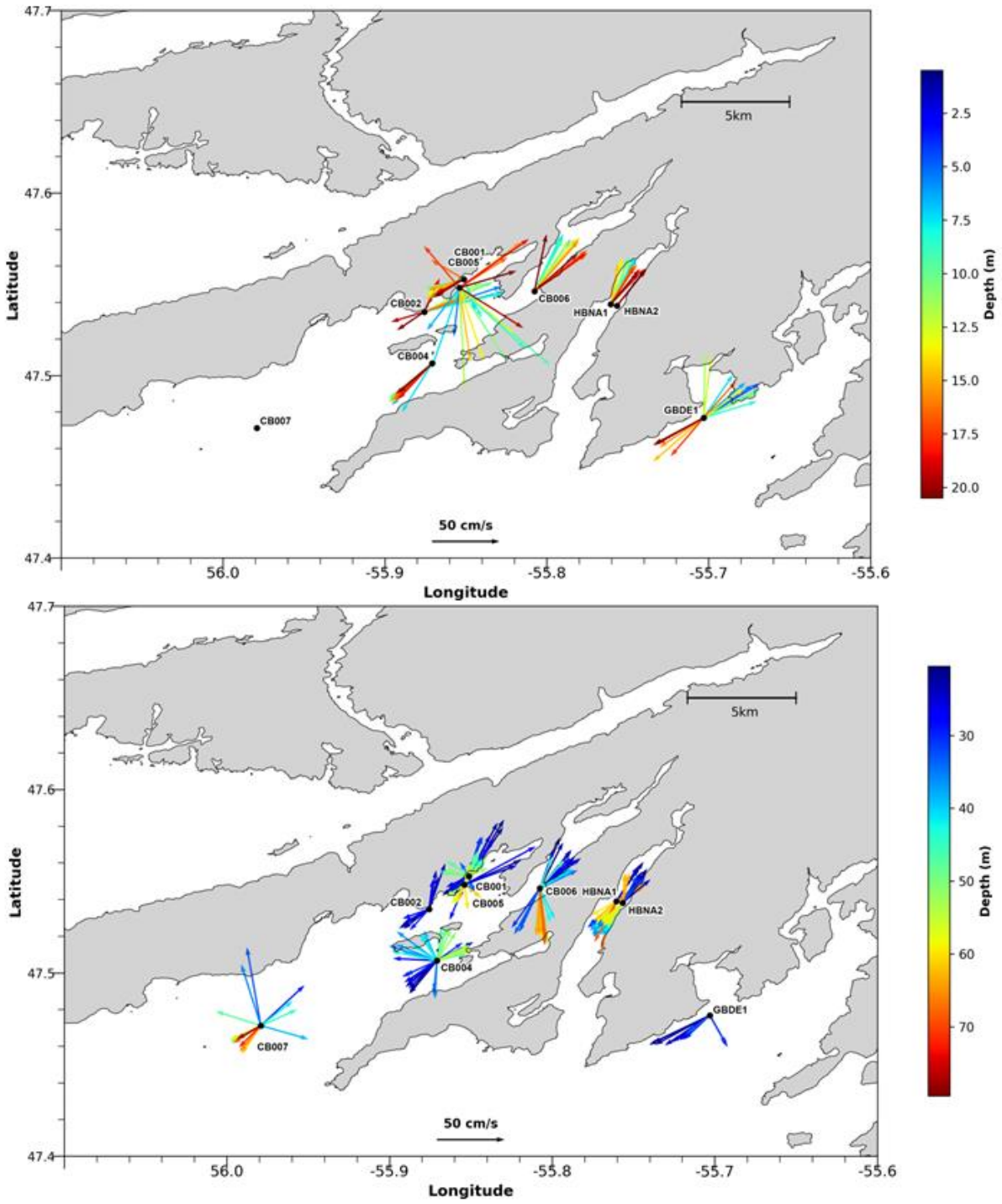

Figure 27. Maximum currents recorded in Connaigre Peninsula for the upper layer (top panel) and for the lower layer (bottom panel).

TIDES

Analysis of the data from the ADCP pressure sensor shows that the five major tidal constituents for sea level are, in order of importance, the semi-diurnal principal lunar M2 (period T=12.42 h), the semi-diurnal principal solar S2 (T=12.00 h), the semi-diurnal larger elliptical lunar N2 (T=12.66 h), the diurnal principal lunar O1 (T=25.82 h), and the diurnal luni-solar declinational K1 (T=23.93 h). This is consistent with the result obtained by analyzing local Canadian Hydrographic Canada (CHS) data (Donnet et al. 2018a) and with previous tidal analyses of other bays located in the southern part of Newfoundland (Han 2000, Ma et al. 2012) and for the northwest Atlantic Ocean in general (Petrie et al. 1987, Han et al. 1996, Han et al. 2010).

Figure 28 illustrates the characteristics of these five major constituents for the Coast of Bays area with a summary given in Table 2. The tidal sea level variability is mainly semi-diurnal with the amplitude of the largest semi-diurnal constituent being almost nine times larger than that of the diurnal ones. The M2 phase computed from all ADCP measurements are relatively consistent (354.9±1.9°) except for two stations which show phases of 0° (BDE21) and ~347° (BB001). Figure 29 illustrates the spatial distribution of the amplitude and phase for M2 computed from the ADCP pressure sensor. The M2 amplitude is larger in BB (generally over 65 cm) than in the other regions and decreases toward the west, consistent with the findings of Donnet et al., 2018a. Smaller M2 amplitudes are found in HB-BDE with values less than 62 cm. Differences are also observed for the phases with BB area showing lower values (less than 355°) and BDE area showing values generally higher (above 355°), except at the mouth of Manual Arm which shows a lower phase (~352°). The differences in phase gives a lag time of ~5.8° (or ~12 min) between the high M2 tide in BDE and that in BB (this lag time becomes ~13°, or ~27 min when considering the outlier phases of BDE21 and BB001).

The amplitude of the other major constituents are significantly smaller than that of M2, three to five times smaller for the semi-diurnal S2 and N2 and nine to eleven times smaller for the diurnal O1 and K1, ratios in line with those computed by Donnet et al. (2018a) using CHS data except for the ratio between M2 and N2 which was slightly higher (5-7 times). The spatial distribution of the amplitude for the other major constituents (Figures in Appendix 4) also shows a tendency to have lower amplitude in HB-BDE and higher amplitude in BB except for N2 for which the amplitudes tend to be lower towards the head of BB. Phase distribution shows a tendency to be slightly higher on the western side (HB-BDE) than on the eastern side (BB).

Looking at the tidal contribution to the sea level variance (Figure 30), the analysis shows a high contribution, with an average of about 83% (ranging from 75% to 93%) when considering all 13 tidal constituents, and an average of about 82% when considering only the five major constituents. Higher contribution is observed in BDE, CP, and then BB with the highest value found at the northern end of Little Passage in the HB-BDE area.

Table 2. Summary (mean and standard deviation) of the major tidal constituents in the Coast of Bays area computed with the ADCP pressure sensor, average amplitude (cm) and phase (degrees).

	M2	S2	N2	O1	K1
Amplitude [cm]	63.4±2.2	17.4±0.9	13.5±1.3	7.2±0.5	5.9±0.5
Phase [degrees]	354.9±1.9	32.1±2.4	335.2±4.7	192.9±4.9	206.2±5.8

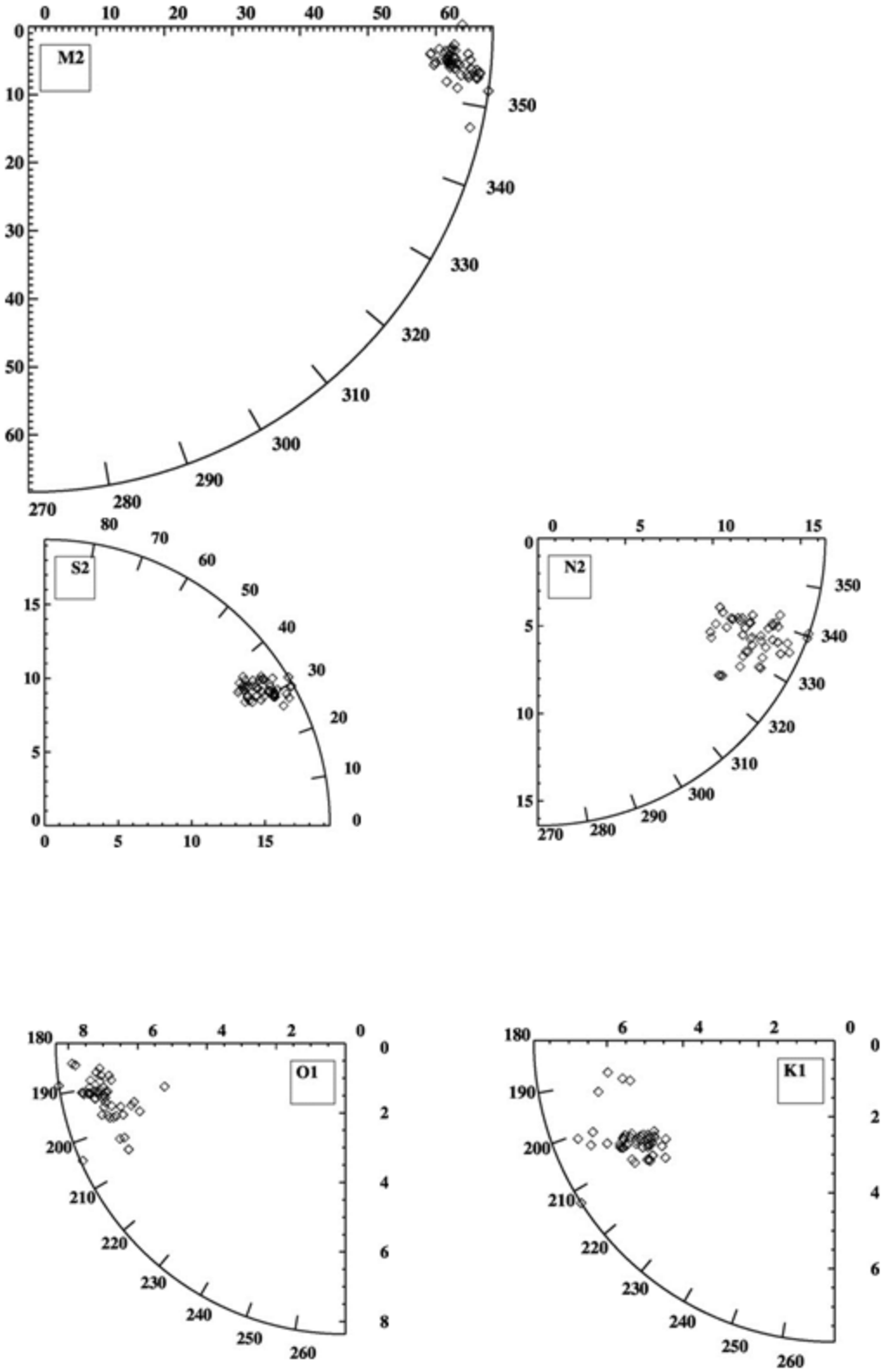

Figure 28. Amplitude [cm] and phase (°) of the main tidal constituents computed from ADCP pressure sensor.

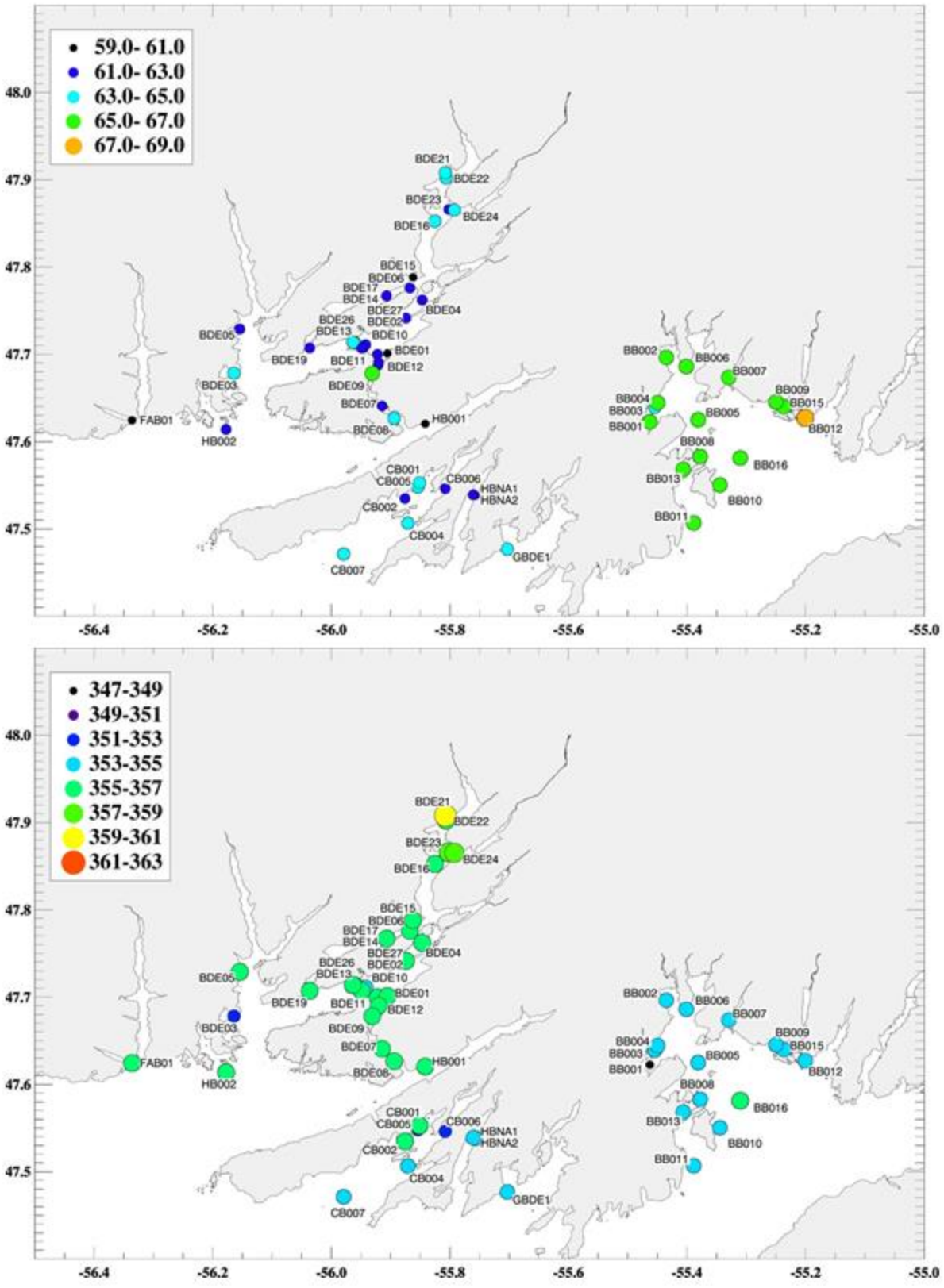

Figure 29. Amplitude in cm (top panel) and phase in degree (bottom panel) of the M2 tides computed from pressure sensor included within the ADCP.

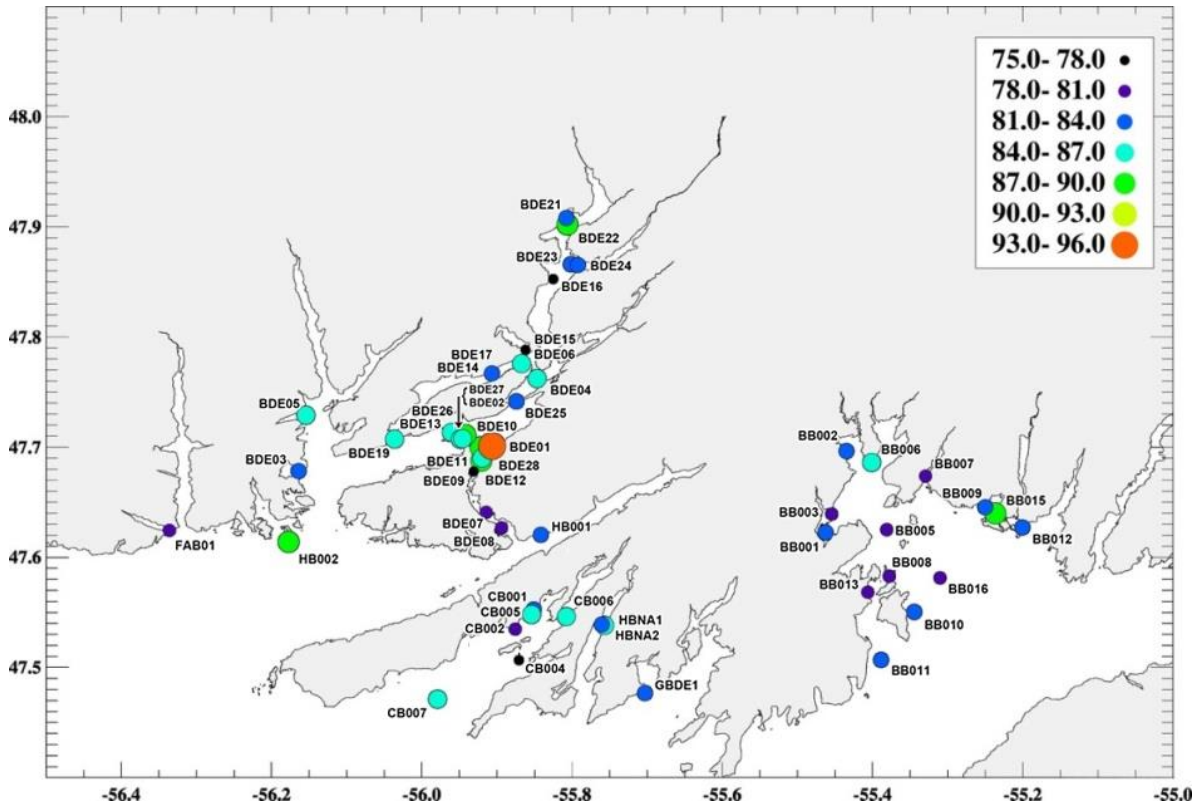

Figure 30. Percentage tidal contribution to sea level variability.

Figure 31 illustrates the maximum speed for the M2 tidal currents and Figure 32 the corresponding tidal ellipse. The tidal analysis was computed using the vertically averaged currents (whole water column). Most of the stations (~88 %) show maximum M2 tidal current speed lower than 6 cm/s. The maximum M2 current speed in the region is about 23 cm/s computed at station BDE24 located towards the head of BDE. The figure also shows that stations with higher maximum M2 currents (larger than 6 cm/s) are found in BDE and stations with lower maximum speed in BB and CP (lower than 3 cm/s). Maximum tidal current speeds from the other major constituents are much smaller (Table 3). Similar to the geographic distribution of M2 tidal currents, stations with higher maximum tidal currents for the other tidal constituents tend to be found in BDE (maps represented in Appendix 5). Tidal signals from the diurnal tidal constituents are relatively small and might be near or below noise level (~1 cm/s). For the inclination, the tidal ellipses generally feel the effect of the bathymetry and follow the direction of the channel where the measurements were carried out.

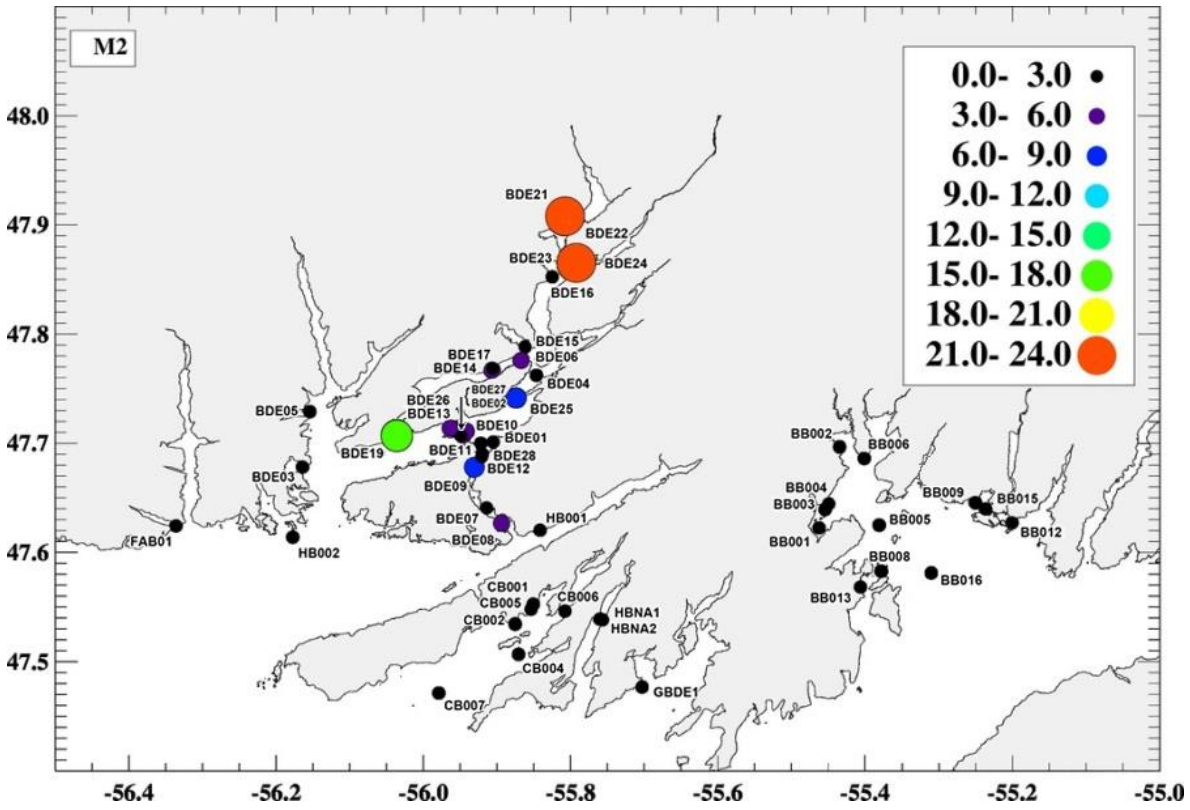

Figure 31. Maximum current speed [cm/s] for M2 tidal currents computed from the vertically averaged currents.

Table 3. Maximum tidal current speeds [cm/s] for the major constituents computed using vertically averaged currents.

-	M2	S2	N2	O1	K1
Speed [cm/s]	23	8	5	1	2

The tidal contribution to currents variance is very different from the contribution to sea level. Figure 33 and Figure 34 present maps of tidal current contribution computed using vertically averaged currents of the upper 20 m and from 20 m to the sea-bottom, respectively. Large differences are observed within HB-BDE and between HB-BDE and the other regions. The following observation can be made

- Within HB-BDE, the tidal current contribution is relatively small (less than 10%) in HB and within Lampidoes Passage but it is larger around Bois Island and in the area towards the head of BDE.
- In the area of BDE with higher tidal contribution, the lower layer presents larger contribution. Maximum contribution is over 50% in the lower layer but up to 40 % in the upper 20 m.

Tidal current contribution (for both the upper and lower layers) is very low in BB and CP regions (with values less than 5% in BB and less than 10% in CP).

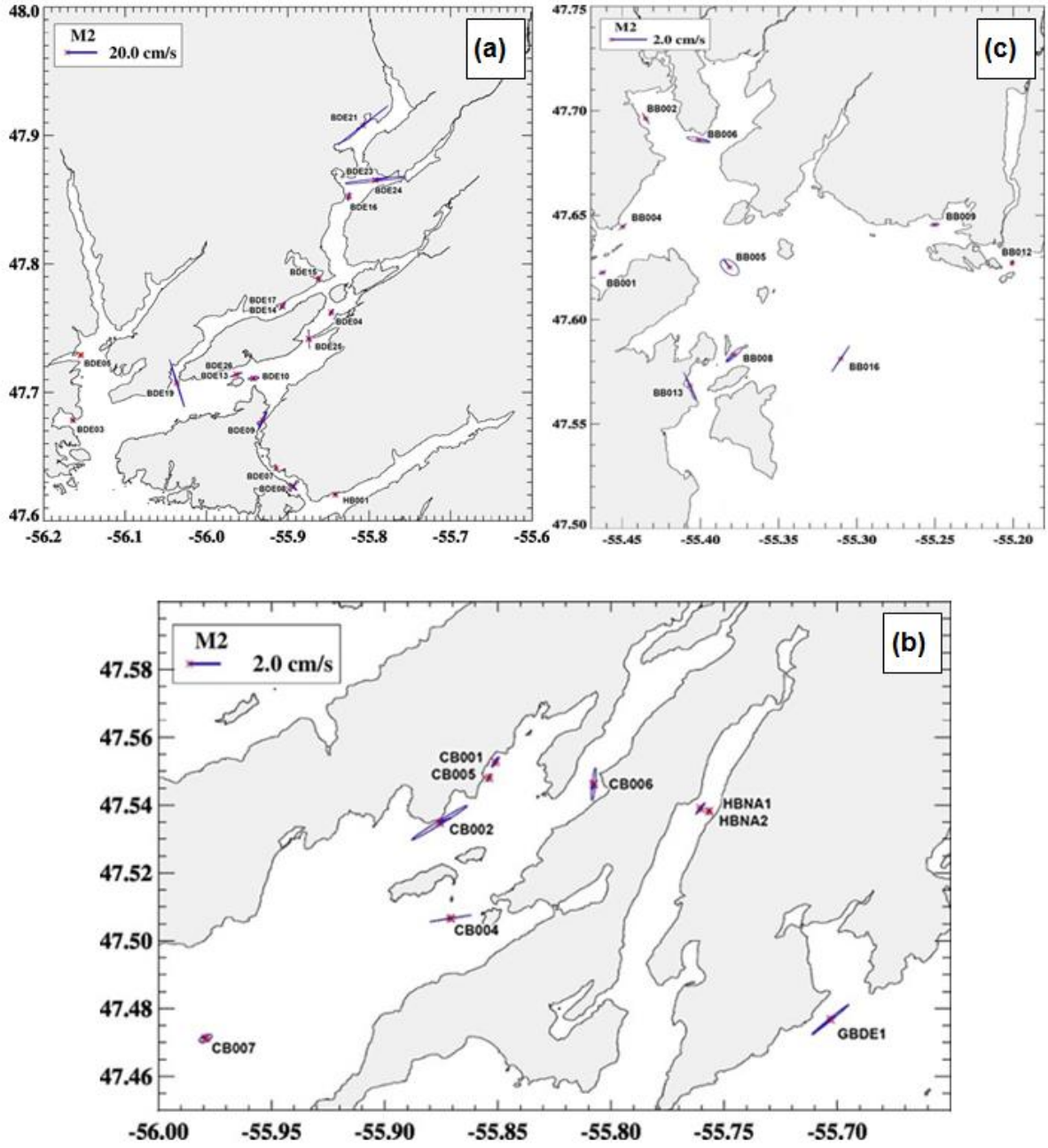

Figure 32. Tidal ellipse for M2 computed from the vertically averaged currents in (a) BDE, (b) CP, and (c) BB. Note the change of scale for BDE region

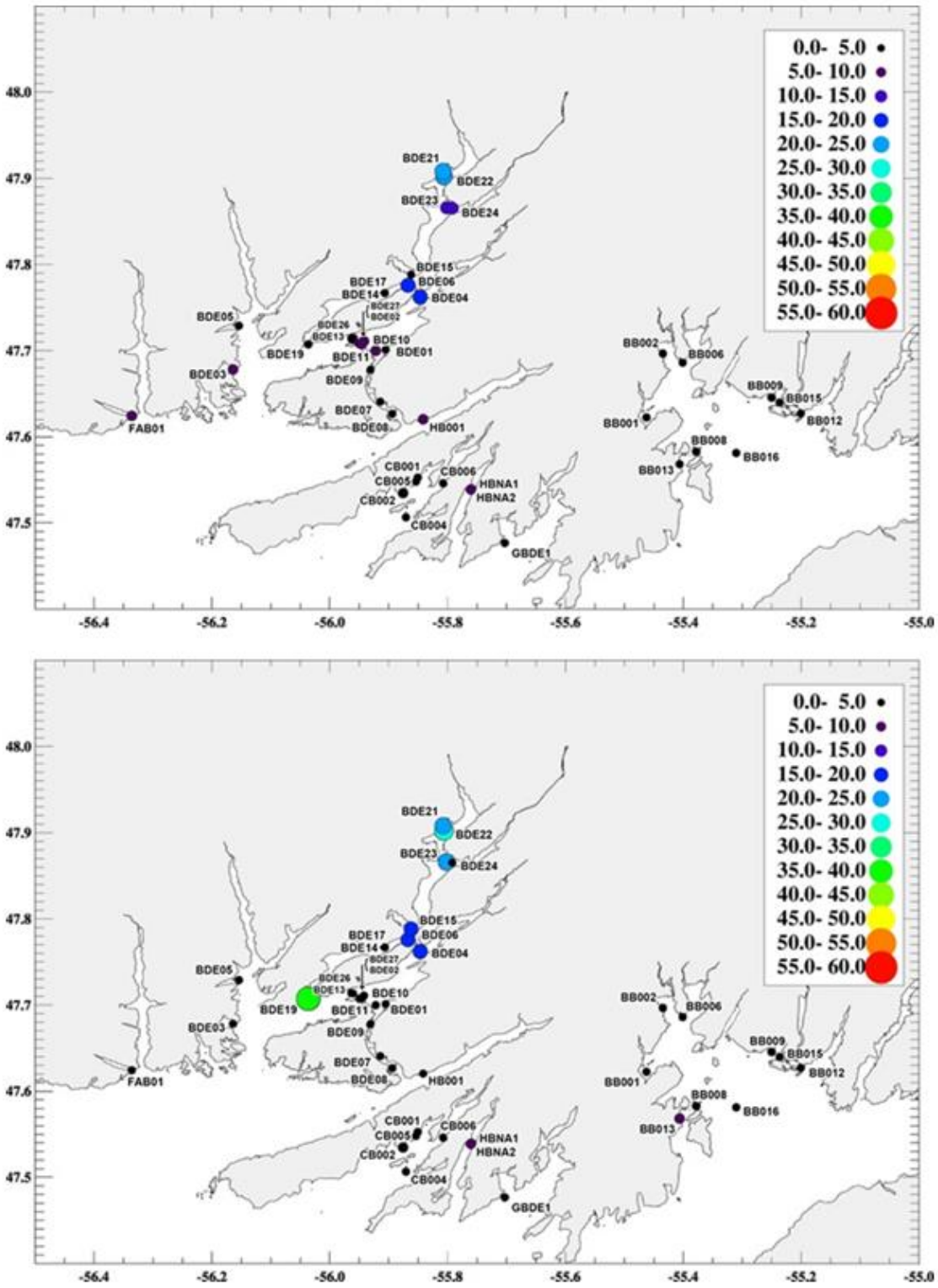

Figure 33. Percentage tidal current contribution in the upper 20 m. Upper panel represents the contribution for the West-to-East component (zonal) of the currents and lower panel the contribution for the South-to-North component (meridional) of the currents.

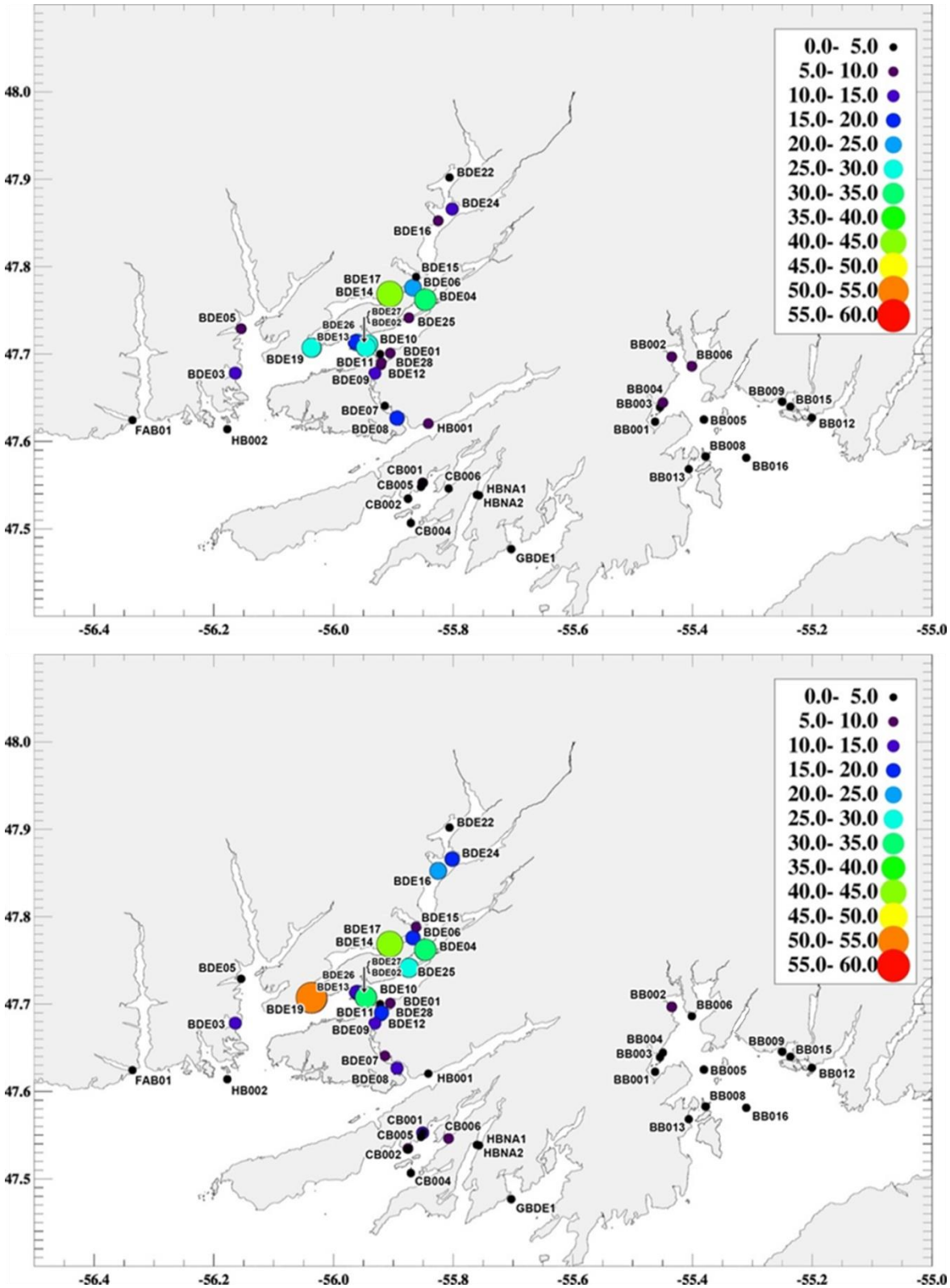

Figure 34. Percentage tidal current contribution for the lower layer (below 20 m depth).Upper panel represents the contribution for the West-to-East component (zonal) of the currents and lower panel the contribution for the South-to-North component (meridional) of the currents.

DISCUSSION

Throughout the analysis, an increase of median current speed from the near surface to deeper depths was observed with the median speed in the layer above 20 m being at least 1.3 times larger than that below 20 m. The median current speed computed for the layer below 20 m depth was in general between ~2 and ~7 cm/s. Above the 20 m depth the median current speed was generally between 2 and 10 cm/s. This later range covers the water layer between 5 and 20 m due to the limitation in the ADCP measurement. It is expected that at the surface, i.e. 0 5 m depth, the current speed will be faster, particularly in BDE due to its shallow pycnocline (Donnet et al. 2018b). Ratsimandresey et al. 2011 reported that during Summer, surface drifter experiments carried out in BDE and in Northeast Arm, the mean speed of water movement at the surface inferred from the drifter displacement generally falls between 10 and 25 cm/s with some deployments showing mean speeds above 40 cm/s. A direct comparison between the two datasets cannot be done due to the differences in the length of the measurements and in the analyses; however, the drifter results do suggest a higher current speed at the surface, consistent with the ADCP results. Further analysis using very near surface current measurements and numerical model simulations will provide a more complete picture of the variation.

Areas with high or low water movement were identified. Comparison with maps of bathymetry of the area (Donnet et al 2018a) showed that higher median speed locations, also associated with higher IQR, are generally found around sills and within narrow channels. This is the result of a local acceleration of the flow due to a decrease in the vertical cross-sectional area through which the water has to flow (e.g., Inall and Gillibrand 2010). These locations also show higher mean current velocity in comparison to locations in the same bay indicating the presence of an average transport of water toward one direction. These locations of higher median speed have been found to show stronger mixing (Donnet et al. 2018b) suggesting the interaction among constricted location, strong currents, and mixing.

On the other hand, the stations with lower median current speed were located within sheltered coves where the median speed was below 3.5 cm/s and often where aquaculture farming takes place. In comparison to other sheltered aquaculture areas, this value is low; for example sheltered areas in Norway showed mean velocities of 10-21 cm/s (Johansson et al. 2007). The low median speed areas in the Coast of Bays also show low IQR suggesting weak circulation in general (e.g. station BDE07 within Little Passage or station BB002 at the head of BB). This weak circulation may affect processes such as water and oxygen renewal (e.g., Burt et al. 2012)

Pycnolines separate the surface zone from the deeper ocean. Donnet et al. 2018b have shown that surface pycnoclines in the region are generally found within the first 20 m from spring to fall except in the CP region where it tends to be deeper (20-40 m). They are particularly strong and shallow in BDE (around 3 m in the upper part). The presence of a strong surface pycnocline provides the necessary physical condition for a distinct water circulation between surface and deeper water (e.g., estuarine circulation). This can explain the differences observed in the current speed with the near surface layer showing higher speed than the deeper one.

The spatial variability of the mean and maximum currents (differences among regions and in the vertical) highlight the presence of different forcings that drive the circulation in the area. Changes in the direction of the mean currents between near surface and deeper layers observed in BDE can be explained by the outflow of freshwater from the Bay D'Espoir Hydroelectric Generating Facility forming an estuarine circulation. Mean current directions are generally more consistent within the whole water column than those of the maximum currents. The former reflects the general circulation in the region and is the result of the different forcing fields and their combination while the latter is in great part due to high wind events (Salcedo-

Castro and Ratsimandresy 2013, Currie et al. 2014, Donnet et al. 2018a). The layering effect is less apparent in BB and CP than in BDE. This might be related to BB and CP being subject to a less freshwater discharge than BDE. Circulation is also less defined and maximum currents are again directed everywhere. Transient high current velocity, mainly within the surface layer, has been observed at most locations of the region. Its occurrence is associated with atmospheric events (e.g. passage of a storm, heavy precipitations) generating oceanographic responses (Salcedo-Castro and Ratsimandresy 2013). Further investigation on the processes that lead to its occurrence will be necessary to quantify its relationship with the forcing events.

From the tidal analysis performed on the sea surface elevation, the results show that the tidal harmonics are in line with previous analyses of tides in the surrounding areas, M2 shows a decrease in amplitude and propagation of the waves from the east to the west with a time lag of ~12 min. between the high tides in the eastern and western side of the region of study. Over the whole area of interest, the variance of the sea level is explained in great part by tides; this is not the case for the currents which show generally low and geographically variable tidal contribution.

Differences in the contribution of the tidal current to the total currents suggest the presence of other more important forces acting in the area. Various types of forces can be involved and their respective role can vary from one location to another and between seasons. Donnet et al. 2018a, 2018b) have reported on the presence of freshwater in the area and its effect on both circulation and water structure (stratification). The freshwater is mainly observed near the surface with stronger signals in BDE than in other bays. Another forcing which also needs consideration is wind. Wind in the region can be very strong (Salcedo and Ratsimandresy 2013, Currie et al. 2014, Donnet et al. 2018a) as seen in wind gust as well as in persistent wind. Donnet et al. 2018a showed that a persisting strong wind with speed of 20 m/s has been observed at Sagona Island for a continuous period of up to 40 hours. The differences in forcing can also be seen in the vertical; for example, at station BDE19, located on a sill at the southern mouth of Lampidoes Passage, the tidal current contribution is less in the upper layer than in the lower layer (below 20 m depth); the mean currents in the upper layer flow out of the bay and those near the bottom into the bay. Given the presence of an outflow of surface brackish water in the region (Donnet et al. 2018a), this suggests a contribution of estuarine circulation at that location in addition to the computed tidal current contribution. Donnet et al 2018a provided a rough estimate of surface currents at 24 cm/s under extreme daily runoff scenario of freshwater from the Bay D'Espoir Hydroelectric Generating Facility, this is of the same order of magnitude as the maximum semi-diurnal (M2) tidal currents computed at the head of BDE (~20 cm/s) and one to two times the wind induced surface water currents (9-18 cm/s) under a mean wind speed of ~9 m/s measured in the region (Donnet et al. 2018a). Maximum currents recorded at that location were also higher than in other regions with speed more than twice the corresponding maximum tidal currents suggesting other processes contributing to such high currents, Inall and Gilibrand 2010 suggested more processes happening at a location above sill resulting from the interplay between geomorphology and environmental forcing. The processes may include windstress, estuarine circulation, internal tide and waves, and mixing to name but a few. From a study around aquaculture sites in Norwegian coastal water, Johansson et al. 2007 reported that the presence of pycnoclines influences the structure of the currents in the vertical showing differences between layers above and below pycnocline. In our area, pycnoclines are present at different depths and with different strength depending on the region and on the season (Donnet et al. 2018b) and will accordingly affect the structure of the currents in the vertical. Thus, quantification of the role of the different forces for each region is necessary to understand the circulation.

The analysis of temporal variability of currents shows that increases of as much as 50% can be seen in the upper layer median currents in fall in comparison to other seasons. Such increases in fall season were also observed with the maximum currents but with even higher rate (~100%). These increases of ocean currents in fall are in line with the increase of wind speed between April and October as reported by Donnet et al 2018a. The high maximum currents, almost five to ten times larger than the median currents, can occur all year long depending on the forces that drive the circulation. These strong currents can last for one day (Salcedo-Castro and Ratsimandresy 2013) and can transport particles far from their emitting locations (e.g. waste particles from aquaculture farms). This leads to the necessity to further understand the main forces and processes that drive such strong currents and how the current circulation responds to them.

The comparison of the map of aquaculture leases in the Coast of Bays area (Figure 1) with our results provides information on the characteristics of the currents within the different lease areas. Fifty-four percent of the lease areas are located in zones where the median current speed is between 4-6 cm/s (for the upper layer); 14% in areas with median speed above 6 cm/s (those that are within Little Passage and in Hermitage Bay) and the other 32% in areas with speeds below 4 cm/s (those mainly found in sheltered coves). Additionally, these lease areas are in zones with low tidal current contributions (less than 10% of contribution) except those that are located in the upper portion of BDE where tidal current contribution reaches values of about 30 % (above 20 m depth). If we consider particle transport due to water movement, a rough estimation can be done using the assumption that the tidal current contribution is very low and that the water moves in the same direction for some time. Such assumption can be made from the fact that for a great part of the measurements, tidal contribution to the currents is less than 10% and that forcing such as freshwater runoff and/or wind can drive the circulation toward specific direction for relatively long periods. An estimate of drifting distance using a 5 cm/s current speed gives ~4.3 km in one day. This is over twice as large as the 2 km distance required in the present application form for aquaculture license. From another point of view it will take 5.5 hours for a particle to reach a distance of 1 km if one considers the 1 km guideline distance between aquaculture farms. These numbers would change under an increased contribution of other forces to drive the water circulation in the area (e.g. wind and freshwater run-off). For example, drifter experiments carried out in the upper portion of BDE showed maximum drifting distance of 12 km in a period of 17 hours, or about 19.6 m/s in mean speed (Ratsimandresy et al. 2012). On the other hand, a hypothetical calculation of particle transport under extreme river runoff within BDE showed that particles could travel up to 53 km in 2.6 days (~24 cm/s, Donnet et al. 2018a). These scales become significant when one considers the potential transport of pathogens, such as virus or parasites, between aquaculture sites or the potential dispersion of waste materials from residential areas to aquaculture sites.

The following limitations are to be considered in the present analysis:

- In the calculation, tidal current contribution was performed for layers generally above 70 m depth (50% of the ADCP were moored at depths between 50-70 m) while the bays are known to be much deeper (Donnet et al. 2018a). Generalization of the estimation of the contribution to circulation in deeper areas should be done with caution as no current measurements were carried out in those areas; tidal contribution should, however, decrease in deeper area unless important internal tide processes take place.
- Given the tendency of the currents to follow the axis of the fjords or channels, the calculation of the tidal current contribution would be better represented after performing a rotation following the principal axis of the current. This can be done after computing the current direction with maximum variance (Thomson and Emery 2014).

- The current speed reported in the present work represents measurements with period ranging from 1 to 6 months of the year. Generalization to annual conditions cannot be done as our analysis does not consider the seasonal variability of the currents due to different forcing such as variability in the wind or variability of freshwater run-off and due to changes in water stratification; which have all been shown to be significant (Donnet et al. 2018a, 2018b)
- Since upward looking ADCP measurements are inherently biased near the surface, only data at the head of Bay d'Espoir provided information in the upper 5 m of the water column, all the other data were measured at depths 5 m or below. Therefore, the statistical summary presented generally reflects current conditions below 5 m depth and information on current conditions near the surface is lacking. The presence of a strong, near surface pycnocline, particularly in BDE area (Donnet et al. 2018b) and the importance of the circulation near the surface for transport of particles to and from aquaculture sites require a better knowledge of the currents at the surface. Our analysis shows that the upper 0-20 m layer presents higher current speed than below 20 m; thus it is expected that currents at the surface (0-5 m) may be faster than what we have reported.
- Uncertainty of the ADCP pressure sensor: according to the manufacturers technical manual (Teledyne RDI 2010a), the short-term uncertainty (i.e., noise) is 0.1% of Full Scale Rating (1 ping). With a sensor's pressure rate of 200 m, the short-term uncertainty is about 20 cm which if applied to a setup of 200 pings/ensemble gives an uncertainty of about 1.4 cm/ensemble. Further uncertainties in the depth calculation occurred since no variation in sea water density were considered (i.e., instrument setup with a constant salinity of 35).

CONCLUSION AND RECOMMENDATION

A statistical analysis of currents at the upper 20 m and those below 20 m is reported together with the characteristics and role of tides in the variation of sea level and variation of currents in the nearshore water of the Coast of Bays area. To the author's knowledge, the present study is the first to give comprehensive information on the current regime and the tidal information of the area. The information can improve our knowledge on topics related to transport of particles from one location to another, including solid and soluble waste to/from aquaculture farms as well as virus and other pathogens present in the area, and knowledge on other topics related to water renewal time in the region (as computed by Donnet et al, 2018a). It also provides information that can be used for aquaculture site selection and site licensing processes. On a larger frame, it extends the general understanding of the tides to regions not covered by earlier large-scale studies such as Han et al. 2010 or Petrie et al. 1987 and expands the results of Donnet et al. (2018a). The circulation model development carried out for the region will also benefits from this information for validation as well as tuning purposes.

Through the analysis, the following key observation can be made:

- The study provides information on the current speed in the Coast of Bays area, the median speed varies between regions ranging from 2.2 to 12.7 cm/s in the upper 20 m and from 1.8 to 13.3 cm/s in the layer below 20 m depth. Variability is found among bays and among the different part of the same bay. Of the three main regions considered in the study, median speeds in the upper and lower layers in Bay d'Espoir are generally the highest and those of Connaigre Bay the lowest.
- Current speed in the upper layer is found to be higher than that in the lower layer. Maximum measured speed was five to ten times larger than the median current speed.

- Water circulation in the area is complex without any dominant pattern besides the BDE estuarine flow and the topographic steering at depths at all sites. Water in the upper 20 m of the water column flows towards the mouth of the fjord in BDE.
- The variability of sea level is well described and is dominated by tides. On average, the tidal contribution explains over 84% of the variance with higher contribution in the Hermitage Bay/Bay d'Espoir region, followed by the Connaigre Peninsula, then Belle Bay region. In contrast, the contribution of the tides to the currents shows a different picture. Only currents in Bay d'Espoir-Lampidoes Passage show notable tidal contribution. The maximum contribution was found at the southern mouth of Lampidoes Passage with a contribution above 55% in the meridional component (S-N) of the velocity when considering the vertically averaged currents of the lower layer (below 20 m depth). The current tidal contribution is generally less than 5% in Belle Bay and less than 10% in the Connaigre Peninsula region.
- In the region of Bay d'Espoir where tidal current contribution is higher, the currents in the upper 20 m of the water column shows less tidal contribution than the whole water column suggesting the presence of other forces that drive the circulation in that layer. In this region the effect of river runoff and wind on the surface circulation is likely more important.
- Median current speed around aquaculture leases is low and generally between 4 and 6 cm/s. Maximum current speeds recorded at these locations is in the same range as those found in the whole bay except for sites with relatively low median current speed (below 3.5 cm/s). At these sites, the maximum recorded current speed was also low suggesting a low energetic environment overall.

Based on the results obtained from the analysis, the following recommendations can be made without any specific order of importance:

- As the surface currents can be faster than what we have reported and are of importance in dispersing and transporting particles to and from aquaculture sites, a better characterization of the currents at the surface will complete the information reported in this work. This can be achieved through complementary surface current measurements with an improved design, acknowledging that such measurements have always been a challenge in coastal and open ocean waters (E.g. Laxague et al. 2018).
- As the water stratification varies due to change in the depth of the pycnocline, further work on analyzing the current regime at different depths in relation to wind conditions and to water stratification will provide better understanding of the variability of the currents that is not explained by tides. A great part of the current variability in Little Passage (BDE), in Belle Bay, and in the Connaigre Peninsula falls in that category.
- Further work will be needed to understand the mechanisms that drive the observed high current speed. Understanding the response time of the water to the driving force as well as the duration of the strong currents will be of importance as they will have an impact on the transport of floating particles within the water column. From a fish health perspective, this short-term temporal variability of the currents can affect processes such as transport and dispersion of pesticides released from tarp or well-boat bath treatment of lice. Knowing where and when the currents will be low or strong can define the timing of the treatment.

ACKNOWLEDGMENTS:

This work was funded by Fisheries and Oceans Canada's Program for Aquaculture Regulatory Research (PARR). The authors also thank Cooke Aquaculture, Northern Harvest Sea Farms,

and the technical staff from the aquaculture and biotechnology section of Fisheries and Oceans Canada for their help and effort in collecting the data.

REFERENCES CITED

Anderson, M.R., Tlusty, M.F., and V.A. Pepper. 2005. Organic Enrichment at Cold Water Aquaculture Sites - the Case of Coastal Newfoundland. Hdb. Env. Chem., Vol. 5, Part M, Environmental Effect of Marine Finfish Aquaculture: 99-113.

Bay D'Espoir Development Association (BDE-DA). 1984. Salmonid Aquaculture in Bay D'Espoir – a Development Plan, Volume III, 133pp.

Boghen, A. D. 1995. Cold Water Aquaculture in Atlantic Canada. 2nd Edition. New Bmnswick: Canadian Institute for Research on Regional Development. xiii + 672p.

Burt, K., Hamoutene, D., Mabrouk, G., Lang, C., Puestow, T., Drover, D., Losier, R. and F. Page. 2012. Environmental conditions and occurrence of hypoxia within production cages of Atlantic salmon on the south coast of Newfoundland. Aquaculture Research, 43: 607–620. doi: 10.1111/j.1365-2109.2011.02867.x.

Chang, B.D., Coombs, K.A., and F.H. Page. 2014. The development of the salmon aquaculture industry in southwestern New Brunswick, Bay of Fundy, including steps toward integrated coastal zone management. *Aquaculture Economics and Management,* 18(1), pp. 1-27.

Currie, J.J., Goulet, P., and A.W. Ratsimandresy. 2014. Wind Conditions in a Fjordlike Bay and Predictions of Wind Speed Using Neighboring Stations Employing Neural Network Models. J. Appl. Meteor. Climatol. 53, 1525-1537.

de Young, B. 1983. Deep water exchange in Fortune Bay, Newfoudland. M.Sc. Thesis, Memorial University of Newfoundland.

Department of Fisheries and Aquaculture (DFA), 2014a. Newfoundland and Labrador Sustainable Aquaculture Strategy 2014. http://www.fishaq.gov.nl.ca/publications/strategicplan/. Accessed on 2 March 2015.

Department of Fisheries and Aquaculture (DFA), 2014b. DFA web site. Statistics – Aquaculture http://www.fishaq.gov.nl.ca/stats/archives/aqua_stats_archive.html. Accessed on 12 March 2015.

Donnet, S., Ratsimandresy, A.W., Goulet, P., Doody, C., Burke, S. and S. Cross. 2018a. Coast of Bays metrics: Geography, Hydrology and Physical Oceanography of an aquaculture area of the South Coast of Newfoundland. DFO Can. Sci. Advis. Sec. Res. Doc. 2017/076. x+109 p.

Donnet, S., Cross, S., Goulet, P., and A.W. Ratsimandresy. 2018b. Coast of Bays seawater vertical and horizontal structure (2009-13): Hydrographic structure, spatial variability and seasonality based on the Program for Aquaculture Regulatory Research (PARR) 2009-13 oceanographic surveys. DFO Can. Sci. Advis. Sec. Res. Doc. 2017/077. viii + 255 p.

Foreman, M.G.G., Chandler, P.C., Stucchi, D.J., Garver, K.A., Guo, M., Morrison, J. and D. Tuele. 2015. The ability of hydrodynamic models to inform decisions on the siting and management of aquaculture facilities in British Columbia. DFO Can. Sci. Advis. Sec. Res. Doc. 2015/005. vii + 49 p.

Foreman, M.G.G., Cherniawsky, J.Y., and V.A. Ballantyne. 2009. Versatile Harmonic Tidal Analysis: Improvements and Applications. *J. Atmos. Oceanic Tech.* 26, 806-817. DOI: 810.1175/2008JTECHO1615.1171.

Golub, G. H., and C. F. Van Loan. 1983. *Matrix Computations*, Johns Hopkins Univ. Press, Baltimore, Md. 476 pp.

Gustafson, L. L., Ellis, S. K., Beattie, M. J., Chang, B. D., Dickey, D. A., Robinson, T. L., Marenghi, F. P., Moffett, P.J., and F. H. Page. 2007. Hydrographics and the timing of infectious salmon anemia outbreaks among Atlantic Salmon (Salmo salar L.) farms in the Quoddy region of Maine, USA and New Brunswick, Canada. Preventive Veterinary Medicine 78:35–56.

Han, G., Ikeda, M., and P. C. Smith. 1996. Oceanic tides over the Newfoundland and Scotian Shelves from TOPEX/POSEIDON altimetry, Atmos. Ocean, 34, 589–604.

Han, G. 2000. Three-dimensional modelling of tidal currents and mixing quantities over the Newfoundland shelf. J. Geophys. Res. 105(C5): 11407–11422.

Han, G., Paturi, S., de Young, B., Yi, S., and C.-K. Shum. 2010. A 3-D data assimilative tide model of the Northwest Atlantic. Atmosphere-Ocean, 48: 39–57.

Helsley, C.E., and J.W.Kim. 2005. Mixing downstream of a submerged fish cage: A numerical study. IEEE Journal of Oceanic Engineering 30(1):12-9.

Inall, M.E., and P.A. Gillibrand. 2010. The physics of mid-latitude fjords: a review. Geological Society, London, Special Publications 2010 (344), 17–33. http://dx.doi.org/10.1144/SP344.3.

Jarp, J. and E. Karlsen,. 1997 Infectious salmon anaemia (ISA) risk factors in sea-cultured Atlantic salmonSalmo salar. Dis. Aquat. Org.28, 79–86

Johansson D., Juell, J.-E., Oppedal, F., Stiansen, J.-E, and K. Ruohonen. 2007. The influence of the pycnocline and cage resistance on current flow, oxygen flux and swimming behaviour of Atlantic salmon (Salmo salar L.) in production cages. Aquaculture 265: 271–287.

Johansson D., Laursen, F., Ferno, A., Fosseidengen, J.E., and P. Klebert. 2014. The Interaction between Water Currents and Salmon Swimming Behaviour in Sea Cages. PLoS ONE 9(5): e97635. doi:10.1371/journal.pone.0097635Golub, G. H., and C. F. Van Loan, 1983: Matrix Computations. The Johns Hopkins University Press, 476 pp.

Joint Government/Industry Working Group (Scotland), & Scotland. (2000). *Final report of the Joint Government/Industry Working Group on infectious salmon anaemia (ISA) in Scotland*. Edinburgh: Scottish Executive.

Laxague, N. J. M., Özgökmen, T.M., Haus, B.K., Novelli, G., Shcherbina, A., Sutherland, P., and J. Molemaker. 2018. Observations of near-surface current shear help describe oceanic oil and plastic transport. Geophysical Research Letters, 45, 245–249. Website.

Ma, Z., Han, G., and B. de Young. 2012. Modelling Temperature, Currents and Stratification in Placentia Bay, Atmosphere-Ocean, 50:3, 244-260, DOI:10.1080/07055900.2012.677413.

Mansour, A., Hamoutene, D., Mabrouk, G., Puestow, T., and E. Barlow. 2008. Evaluation of some environmental parameters for salmon aquaculture cage sites in Fortune Bay, Newfoundland: emphasis on the occurrence of hypoxic conditions. Can.Tech.Rep.Fish.Aquat.Sci. 2814: vi + 21 p.

Murray, A.G. 2003. The epidemiology of infectious salmon anemia in Scotland. In *International response to infectious salmon anemia: prevention, control, and eradication*: proceedings of a symposium; 3-4 September 2002; New Orleans, LA. Technical Coordinators - O. Miller and R.C. Cipriano. Tech. Bull. 1902. Washington, DC: U.S. Dept, of Agriculture, Animal and Plant Health Inspection Service; U.S. Dept, of the Interior, U.S. Geological Survey; U.S. Dept, of Commerce, National Marine Fisheries Service, p. 55-62. (Available at: https://www.aphis.usda.gov/animal_health/animal_dis_spec/aquaculture/downloads/isa-proceedings.pdf) (accessed 18 September 2018)

Marine Science Research Laboratory (MSRL). 1980. Bay d'Espoir Aquaculture Feasibility Study, Volume II, Section 10: Coastal and Estuarine Pen Rearing Sites, pp 1–37.

McClure C.A., Hammell, K.L., and I.R. Dohoo. 2005. Risk factors for outbreaks of infectious salmon anemia in farmed Atlantic salmon,Salmo salar. Preventive Veterinary Medicine 72,263–280

Oppedal, F., Dempster, T., and L. Stien, 2011. Environmental drivers of Atlantic salmon behaviour in sea-cages: a review. Aquaculture 311, 1–18.

Page, F.H., Chang, B.D., Losier, R.J., Greenberg, D.A., Chaffey, J.D., and E.P. McCurdy. 2005. Water circulation and management of infectious salmon anemia in the salmon aquaculture industry of southern Grand Manan Island, Bay of Fundy. Can. Tech. Rep. Fish. Aquat. Sci. 2595 iii + 78p.

Pepper, V.A., Nicholls, T., Collier, C., Watkins, V., Barlow, E., and M.F. Tlusty. 2003. Quantitative performance measurement of alternative North American salmonid strains for Newfoundland aquaculture. Can. Tech. Rep. Fish. Aquat. Sci. 2502: vi + 53p.

Pepper, V.A., Withler, R., Nicholls, T., and C. Collier. 2004. Quantitative marine performance evaluation of a Newfoundland Atlantic salmon strain for Bay d'Espoir aquaculture. Can. Tech. Rep . Fish. Aquat. Sci. 2540: vii + 44 p.

Petrie, B., Lank, K., and S. de Margerie. 1987. Tides on the Newfoundland grand banks, Atmosphere-Ocean, 25:1, 10-21

Petrie, B., Drinkwater, K., Gregory, D., Pettipas, R., and A. Sandstrom. 1996a. Temperature and salinity atlas for the Scotian Shelf and the Gulf of Maine. Can. Tech. Rep. Hydrogr. Ocean Sci. 171: v + 398 pp.

Petrie, B., Drinkwater, K., Sandstrom, A., Pettipas, R., Gregory, D., Gilbert, D., and P. Sekhon. 1996b. Temperature, salinity and sigma-t atlas for the Gulf of St. Lawrence. Can. Tech. Rep. Hydrogr. Ocean Sci. 178: v + 256 pp.

Press, W.H., Teukolsky, S.A., Vetterling, W.T., and B.P. Flannery. 1992. Numerical Recipes in FORTRAN: The Art of Scientific Computing. Cambridge University Press, Cambridge, U. K

Ratsimandresy, A.W., Page, F., Mabrouk, G., Losier, R., Drover, D., Ings, D., and P. McCurdy. 2012. Aquaculture Drifter Programme: Progress Update 2010. DFO Can. Sci. Advis. Sec. Res. Doc. 2011/127. vi + 41 p.

Richard, J.M., and A.E. Hay. 1984. The physical oceanography of Bay d'Espoir, Newfoundland. Institute of Cold Ocean Sciences. Memorial University of Newfoundland, St. John's, NL, 30pp.

Salcedo-Castro, J., and A.W. Ratsimandresy. 2013. Oceanographic response to the passage of hurricanes in Belle Bay, Newfoundland. Estuarine, Coastal and Shelf Science. 133: 224-234.

Statistics Canada .2013, July 23. Constructing box and whisker plots. Retrieved from http://www.statcan.gc.ca/edu/power-pouvoir/ch12/5214889-eng.htm.

Taylor, V.R. 1975. A Preliminary Assessment of Newfoundland Near-Shore Areas as Potential Sites for Salmonid Mariculture. Environment Canada, Fisheries and Marine Service, Internal Report Series No. NEW /1-75-5 Newfoundland Region.

Teledyne RDI, Inc. 2010a. *WorkHorse Commands and Output Data Format.* P/N 957-6156-00.

Teledyne RDI, Inc. 2011. *Acoustic Doppler Current Profiler Principles of Operation A Practical Primer*. P/N 951-6069-00.

Thomson and Emery, 2014, Data Analysis Methods in Physical Oceanography, 3rd Edition. p 728.

Tlusty, M.F., Pepper, V.A., and M.R. Anderson. 1999. Environmental monitoring of finfish aquaculture sites in Bay d'Espoir Newfoundland during the winter of 1997. Can. Tech. Rep. Fish. Aquat. Sci. No. 2273: vi + 34p.

Upton, G., and I. Cook. 1996. *Understanding Statistics*. New York, NY: Oxford University Press.

Vågsholm, I., Djupvik, H.O., Willumsen, F.V., Tveit, A.M., and K. Tangen. 1994. Infectious salmon anaemia (ISA) epidemiology in Norway. Prev. Vet. Med.19, 277–290. (doi:10.1016/0167-5877(94)90095-7).

Venayagamoorthy, S.K., Ku, H., Fringer, O.B., Chiu, A., Naylor, R.L., and J.R. Koseff. 2011. Numerical modelling of aquaculture dissolved waste transport in a coastal embayment. Environmental Fluid Mechanics.

APPENDIX I

LOCATION, DATES, AND DEPTHS OF THE ADCP DEPLOYMENTS

Station	Bay	Position	Date	Deployment Length [days]	1st cell [m depth]	Deepest cell [m above sea bottom]	Site depth [m]	Percent of water column surveyed
BB001	BB	47.6225N 55.4626W	22 Apr – 20 Jun 2009	59	5	5	50	82
BB002	BB	47.6963N 55.4349W	20 Jun – 25 Sep 2009	97	5	5	42	79
BB002	BB	47.6968N 55.4349W	25 Sep – 5 Nov 2009	41	6	6	52	79
BB003	BB	47.6392N 55.4544W	15 Oct 2010 – 14 Apr 2011	181	39	6	75	41
BB004	BB	47.6444N 55.4497W	6 May – 30 Jun 2011	55	37	6	97	57
BB005	BB	47.6250N 55.3812W	6 May – 29 Jun 2011	54	32	66	147	34
BB005	BB	47.6249N 55.3809W	3 Jul – 22 Oct 2011	111	6	70	152	51
BB006	BB	47.6861N 55.4012W	7 May – 30 Jun 2011	54	6	6	61	82
BB007	BB	47.6737N 55.3296W	7 May – 29 Jun 2011	53	-	-	73	-
BB008	BB	47.5827N 55.3783W	7 May – 30 Jun 2011	54	7	6	60	80
BB008	BB	47.5827N 55.3784W	30 Jun – 24 Oct 2011	116	7	6	59	80
BB008	BB	47.5827N 55.3784W	24 Oct 2011 - 25 Feb 2012	124	7	6	59	80
BB009	BB	47.6454N 55.2500W	8 May – 29 Jun 2011	52	6	6	57	81
BB009	BB	47.6453N 55.2500W	1 Jul – 15 Oct 2011	106	7	6	53	77
BB009	BB	47.6454N 55.2500W	22 Oct 2011 - 20 Feb 2012	121	16	6	65	68
BB009	BB	47.6456N 55.2506W	26 Sep - 24 Oct 2012	28	7	6	57	79
BB010	BB	47.5503N 55.3444W	30 Jun – 20 Oct 2011	112	-	-	61	-
BB011	BB	47.5068N 55.3887W	30 Jun – 22 Oct 2011	114	-	-	69	-
BB012	BB	47.6271N 55.2006W	1 Jul – 23 Oct 2011	114	15	6	74	73
BB013	BB	47.5682N 55.4065W	22 Sep – 22 Oct 2011	51	4	6	35	74
BB015	BB	47.6397N 55.2365W	1 May – 19 Aug 2012	110	6	6	56	80
BB016	BB	47.5812N 55.3102W	26 Sep – 24 Oct 2012	28	7	6	56	79
BDE01	BDE	47.7010N 55.9051W	25 Apr – 13 Jul 2010	79	5	5	40	78

Station	Bay	Position	Date	Deployment Length [days]	1st cell [m depth]	Deepest cell [m above sea bottom]	Site depth [m]	Percent of water column surveyed
BDE02	BDE	47.7076N 55.9459W	21 Apr – 16 Jun 2009	56	7	6	67	82
BDE03	BDE	47.6782N 56.1641W	22 Apr – 15 Jun 2009	54	5	6	50	80
BDE04	BDE	47.7622N 55.8466W	17 Jun – 23 Sep 2009	98	7	6	58	79
BDE05	BDE	47.7289N 56.1543W	17 Jun – 23 Sep 2009	98	16	5	57	65
BDE06	BDE	47.7758N 55.8672W	23 Jun – 22 Sep 2009	91	4	5	28	71
BDE07	BDE	47.6408N 55.9142W	24 Sep – 5 Nov 2009	42	5	5	36	75
BDE08	BDE	47.6266N 55.8940W	24 Sep – 5 Nov 2009	42	8	6	71	82
BDE09	BDE	47.6780N 55.9309W	26 Sep – 5 Nov 2009	40	5	5	48	81
BDE10	BDE	47.7109N 55.9421W	25 Apr – 13 Jul 2010	79	7	6	73	84
BDE11	BDE	47.6998N 55.9220W	25 Apr – 12 Jul 2010	78	7	56	121	49
BDE12	BDE	47.6876N 55.9208W	26 Apr – 12 Jul 2010	77	49	56	154	32
BDE13	BDE	47.7134N 55.9606W	26 Apr – 13 Jul 2010	78	7	6	66	82
BDE14	BDE	47.7669N 55.9068W	13 Jul – 13 Oct 2010	92	6	6	57	81
BDE15	BDE	47.7882N 55.8620W	15 Oct 2010-10 Mar 2011	146	6	6	44	75
BDE16	BDE	47.8525N 55.8252W	15 Oct 2010 - 3 Mar 2011	138	42	6	75	37
BDE17	BDE	47.7685N 55.9060W	5 May – 28 Jun 2011	54	29	6	75	55
BDE19	BDE	47.7072N 56.0364W	2 May – 2 Aug 2012	92	6	6	60	82
BDE19	BDE	47.7073N 56.0366W	23 Sep – 18 Nov 2012	56	7	6	59	80
BDE19	BDE	47.7073N 56.0368W	27 Apr – 9 Jul 2013	73	6	6	45	76
BDE19	BDE	47.7068N 56.0362W	9 Jul – 17 Oct 2013	100	6	6	54	80
BDE21	BDE	47.9079N 55.8076W	3 May – 13 Sep 2012	133	1	3	10	62
BDE22	BDE	47.9020N 55.8062W	3 May – 17 Aug 2012	106	5	6	44	77
BDE23	BDE	47.8659N 55.8017W	3 May – 12 Aug 2012	100	6	6	59	81
BDE24	BDE	47.8652N 55.7923W	25 Apr – 9 Jul 2013	75	1	3	9	64
BDE24	BDE	47.8653N 55.7920W	11 Jul – 17 Oct 2013	98	1	3	10	58

Station	Bay	Position	Date	Deployment Length [days]	1st cell [m depth]	Deepest cell [m above sea bottom]	Site depth [m]	Percent of water column surveyed
BDE25	BDE	47.7414N 55.8741W	21 Sep – 18 Nov 2012	58	41	6	88	48
BDE26	BDE	47.7138N 55.9634W	22 Sep – 18 Nov 2012	57	7	6	63	81
BDE26	BDE	47.7138N 55.9634W	26 Apr – 9 Jul 2013	74	6	6	67	84
BDE26	BDE	47.7139N 55.9636W	11 Jul – 17 Oct 2013	98	44	6	79	38
BDE26	BDE	47.7138N 55.9634W	18 Oct 2013 - 10 Jun 2014	235	4	46	68	28
BDE27	BDE	47.7071N 55.9487W	22 Sep – 18 Nov 2012	57	8	6	73	82
BDE27	BDE	47.7074N 55.9497W	26 Apr – 9 Jul 2013	74	6	6	74	85
BDE27	BDE	47.7075N 55.9488W	11 Jul – 17 Oct 2013	98	37	6	71	41
BDE28	BDE	47.6899N 55.9200W	26 Apr – 9 Jul 2013	74	-	-	63	-
BDE28	BDE	47.6899N 55.9198W	11 Jul – 8 Oct 2013	89	-	-	69	-
CB001	CB	47.5527N 55.8511W	18 Jun – 14 Jul 2012	26	7	6	61	80
CB001	CB	47.5527N 55.8506W	14 Jul – 6 Oct 2012	84	7	6	68	82
CB002	CB	47.5348N 55.8757W	14 Jul – 4 Nov 2012	113	5	5	36	75
CB002	CB	47.5342N 55.8754W	19 Nov 2012 - 14 Mar 2013	115	7	6	57	79
CB004	CB	47.5066N 55.8708W	19 Nov 2012 - 28 Mar 2013	129	7	6	62	81
CB005	CB	47.5480N 55.8539W	23 Apr – 10 Jul 2013	78	8	6	73	82
CB005	CB	47.5484N 55.8542W	10 Jul – 16 Oct 2013	98	7	6	63	81
CB005	CB	47.5481N 55.8538W	4 Nov 2013 - 6 Jun 2014	214	9	6	70	80
CB005	CB	47.5489N 55.8540W	6 Jun – 6 Sep 2014	92	7	6	65	82
CB006	CB	47.5461N 55.8076W	23 Apr – 10 Jul 2013	78	10	6	76	80
CB006	CB	47.5462N 55.8077W	10 Jul – 17 Oct 2013	98	7	6	75	84
CB006	CB	47.5462N 55.8080W	16 Oct 2013 - 8 May 2014	204	17	6	76	71
CB006	CB	47.5462N 55.8078W	8 May – 6 Sep 2014	121	8	6	73	82
CB007	CB	47.4712N 55.9791W	4 May – 16 Oct 2013	165	32	8	87	55
FAB01		47.6244N 56.3360W	18 Jul – 16 Nov 2012	121	7	6	63	81

Station	Bay	Position	Date	Deployment Length [days]	1st cell [m depth]	Deepest cell [m above sea bottom]	Site depth [m]	Percent of water column surveyed
GBDE1	CB	47.4767N 55.7030W	14 Jul – 12 Oct 2010	90	5	5	39	77
HB001	HB	47.6205N 55.8416W	13 Jul – 13 Oct 2010	92	6	6	58	81
HB002	HB	47.6139N 56.1775W	2 May – 13 Aug 2012	103	30	6	68	49
HBNA1	CB	47.5390N 55.7605W	14 Jul – 12 Oct 2010	90	7	6	75	84
HBNA2	CB	47.5381N 55.7566W	14 Jul – 12 Oct 2010	90	20	6	70	64

APPENDIX II

GANTT CHART SHOWING THE PERIOD OF MEASUREMENT OF EACH ADCP STATION

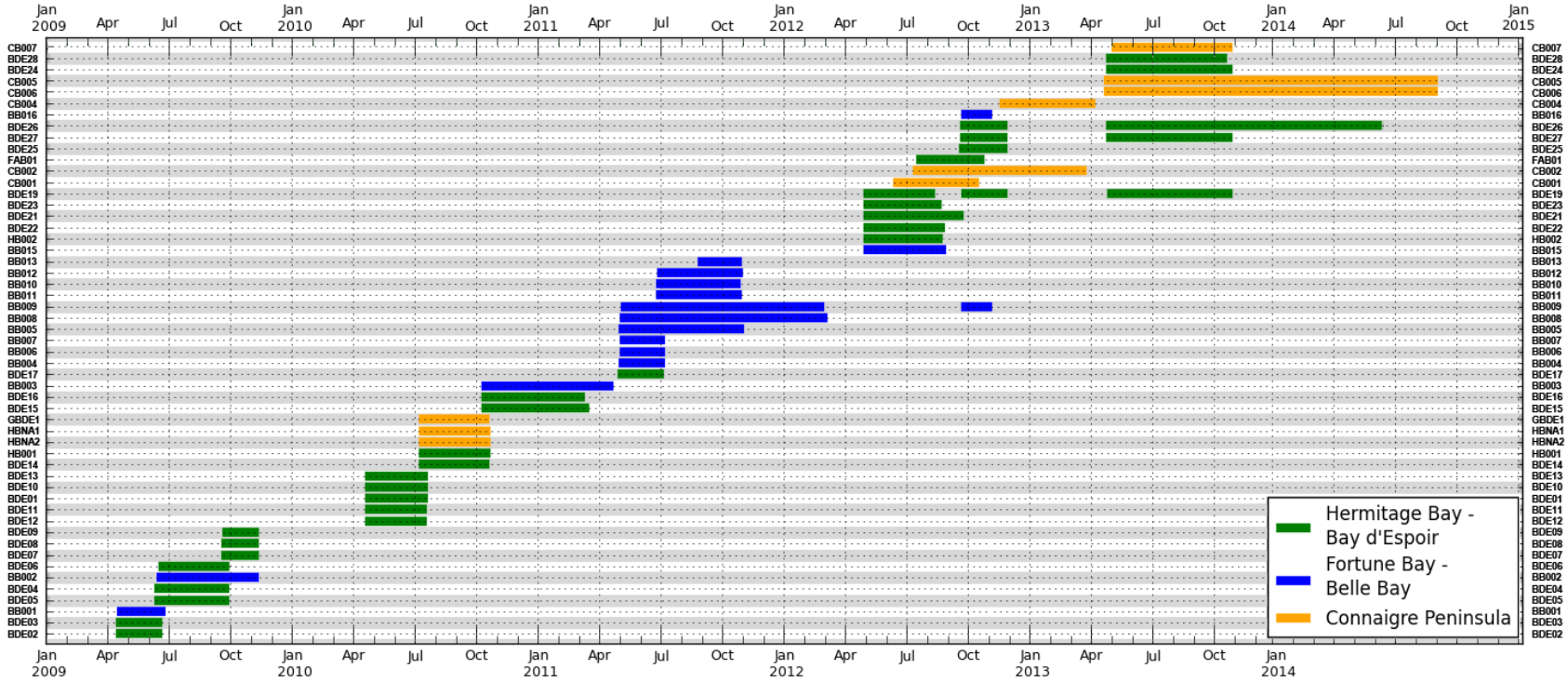

APPENDIX III

HISTOGRAM SHOWING THE DIFFERENCES BETWEEN THE MAXIMUM CURRENT SPEEDS IN THE UPPER LAYER AND THOSE IN THE LOWER LAYER.

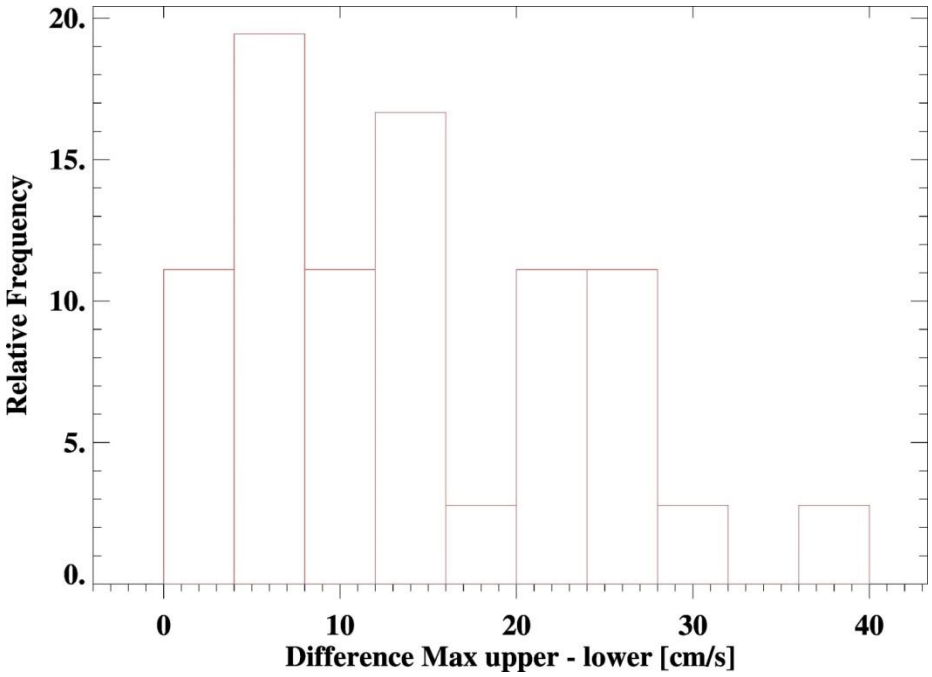

APPENDIX IV

Maps of amplitude and phase for S2, N2, O1, and K1 constituents in the Coast of Bays area.

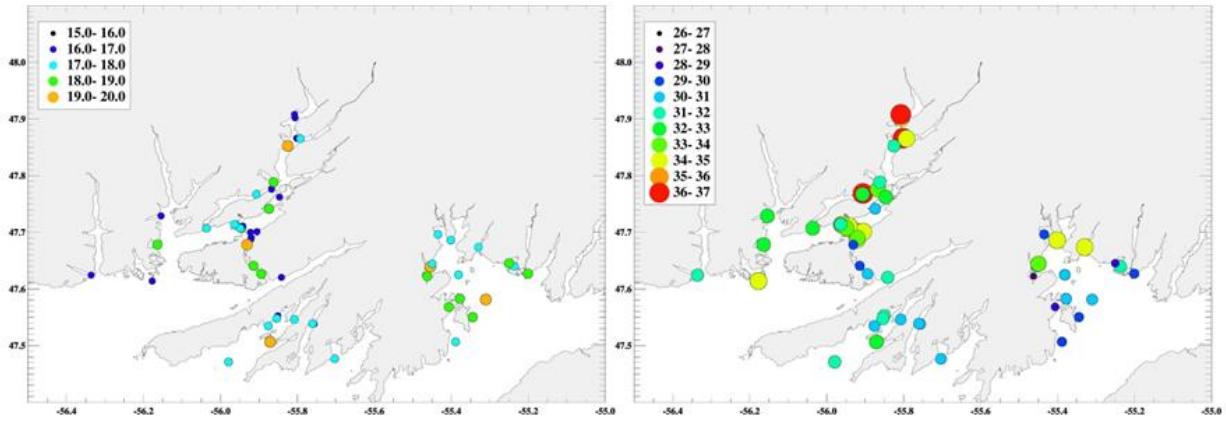

Amplitude [cm] and phase [°] of the S2 tides computed from ADCP pressure sensor.

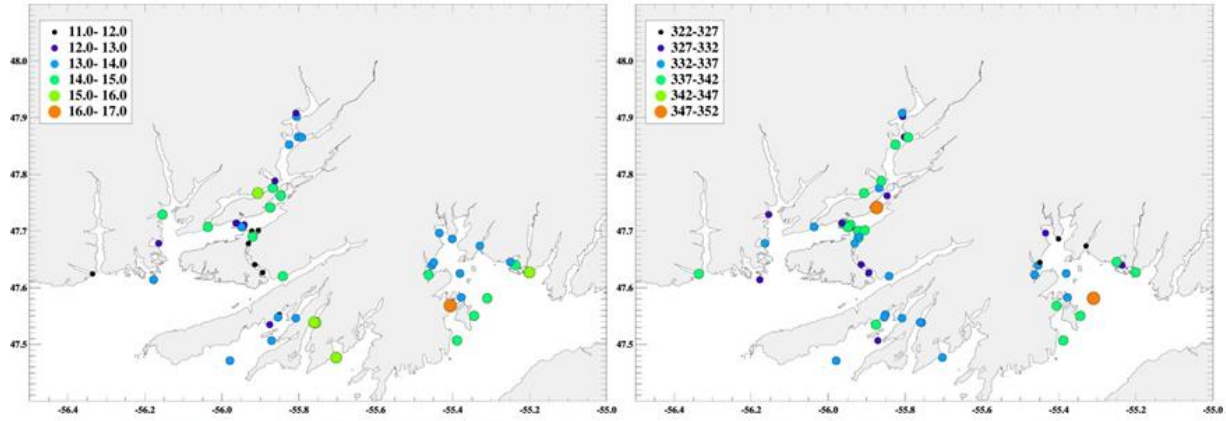

Amplitude [cm] and phase [°] of the N2 tides computed from ADCP pressure sensor.

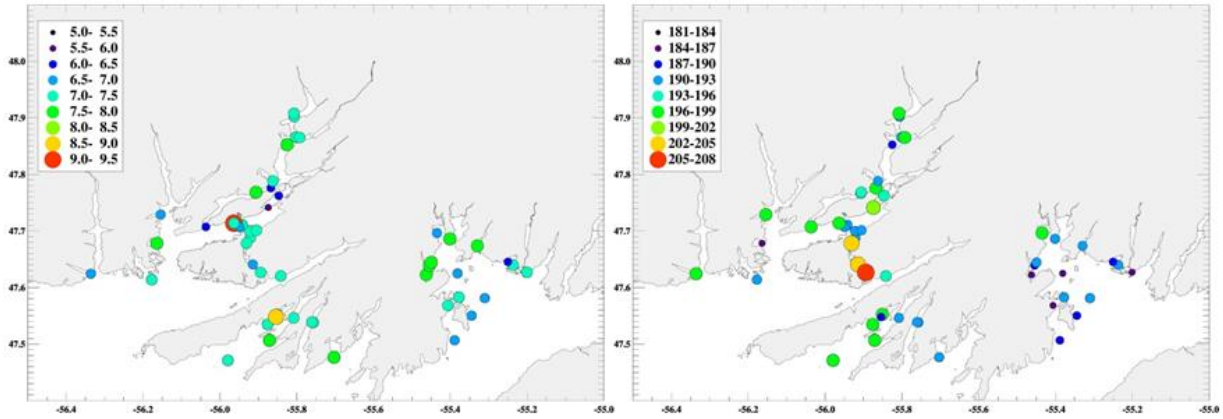

Amplitude [cm] and phase [°] of the O1 tides computed from ADCP pressure sensor.

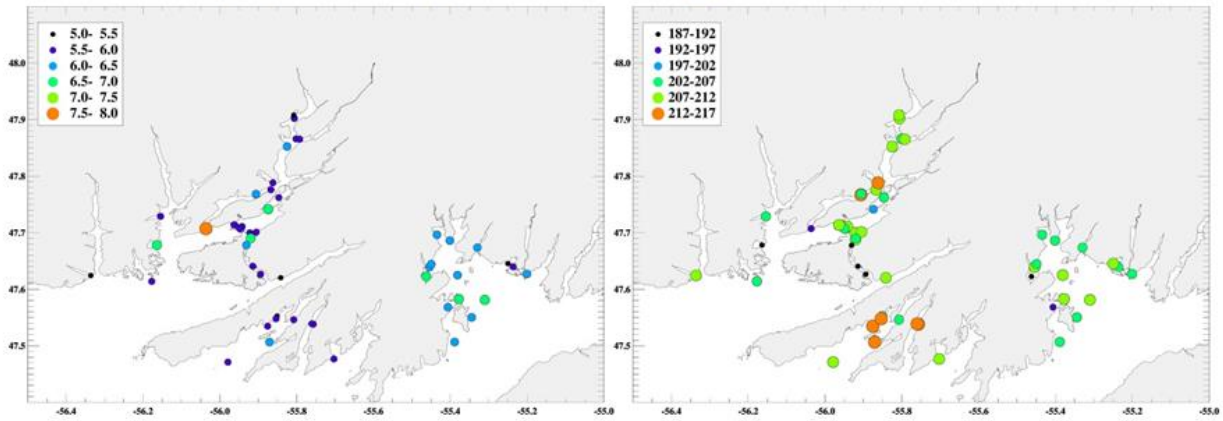

Amplitude [cm] and phase [°] of the K1 tides computed from ADCP pressure sensor.

APPENDIX V

MAPS OF THE MAXIMUM SPEED FOR THE MAIN TIDAL CONSTITUENTS (S2, N2, K1, O1)

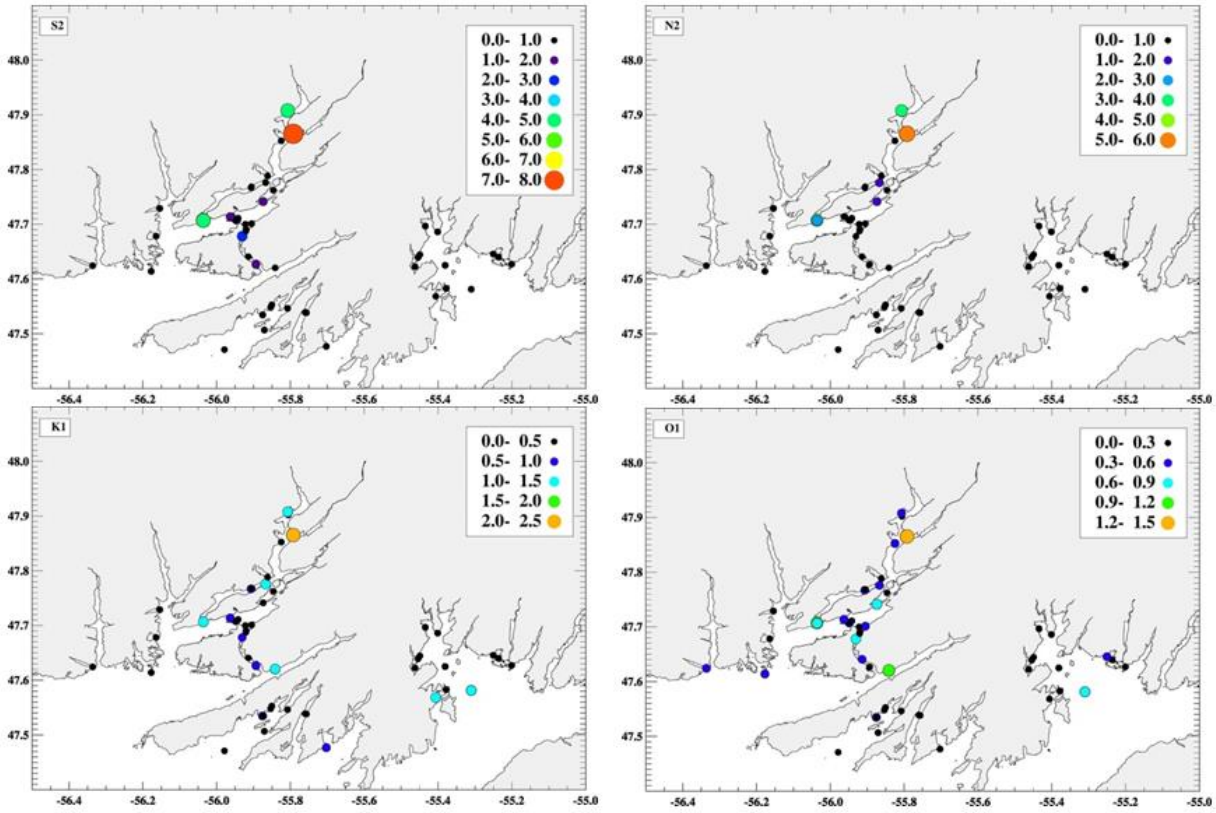

Maximum tidal current speed [cm/s] for the main tidal constituents (S2, N2, K1, and O1) computed from the vertically averaged currents over the whole water column.